The role of cave ventilation in the triple oxygen and hydrogen isotope composition of condensation waters in Altamira Cave, northern Spain

Fernando Gázquez[1,2*], Luis Quindós[3,4], Daniel Rábago[3], Ismael Fuente[3], Santiago Celaya[3], Carlos Sainz[3,4]

(1) Department of Biology and Geology, Universidad de Almería, Carretera de Sacramento s.n, La Cañada de San Urbano, Almería, 04120, Spain.

(2) Andalusian Centre for the Monitoring and Assessment of Global Change (CAESCG), University of Almería, Spain

(3) Radon Research Group. Faculty of Medicine. University of Cantabria, Avda. Cardenal Herrera Oria s/n E-39011 Santander, Spain.

(4) The Cantabrian International Institute for Prehistoric Research (IIIPC)

*Corresponding author (f.gazquez@ual.es)

Abstract

In cave environments, water vapor condensation occurs naturally when warmer/wet air masses flow close to colder cave surfaces. Artificial microclimate perturbations in show caves can enhance this process, leading to potential deterioration of rock art and degradation of speleothems. Here we investigate the triple oxygen and hydrogen isotopic compositions of condensation water in Altamira Cave (Cantabria, northern Spain) to evaluate the potential of stable isotopes in the study of condensation mechanisms in caves. We assess the role of cave ventilation in the spatiotemporal isotopic variability of condensation water in Altamira Cave. To this end, water drops that condense naturally on artificial supports in different parts of the cave were

collected for 7 years and their isotopic compositions ($\delta^{17}O$, $\delta^{18}O$, δD and derived parameters ^{17}O-excess and d-excess) were compared to those of droplets with no apparent dripping taken from the cave ceiling (i.e. presumably condensation water) and fast dripping points (i.e. infiltration water) during the same period. Condensation waters in the outmost cave sectors, closer to the entrance, show higher $\delta^{17}O$, $\delta^{18}O$ and δD values during the cave ventilation period (June to October) compared to the rest of the year. This seasonal pattern can be explained by changes in the contributions of two moisture sources for condensation: advection of allochthonous water vapor from outside during the cave ventilation period and recycling of autochthonous vapor generated from cave dripwater during the stagnation period. In contrast, the isotopic values of condensation waters in the inner cave sectors are similar to those of infiltration water, with insignificant seasonal variability. This suggests that water condensation in the inner cave sectors is sourced by autochthonous vapor, with no significant contributions of external moisture, even during the cave ventilation period. We conclude that allochthonous water vapor condenses preferentially in the *Entrance Hall* and does not affect significantly the rest of the cave. These results are relevant for the management of Altamira Cave and for future investigations on condensation mechanisms in cavities elsewhere.

Keywords: cave management, cave monitoring, condensation water, stable isotopes, oxygen-17, triple oxygen isotopes.

1. Introduction

The prehistoric paintings of the *Polychrome Hall* of Altamira Cave are the maximum expression of the Paleolithic rock art in the Iberian Peninsula. This cave hosts

49 priceless rock art paintings, some 36,160 – 15,329 cal. BP that have earned it the
50 name “Sistine Chapel” of the Paleolithic, due to the reddish and ochre-colored bison
51 and deer paintings that cover the ceiling of the renowned *Polychrome Hall* (Pike et al.,
52 2012; Gázquez et al., 2017a) (Fig. 1). The cave was declared World Heritage Site by
53 the UNESCO in 1985 (http://whc.unesco.org/en/list/310) and was recently reopened
54 to the public under an extremely restrictive visitor regime (Gázquez et al., 2016, 2017a;
55 Sainz et al., 2017). Preserving the integrity of these and others rock art features from
56 natural and anthropic perturbations is a priority in the management of show caves.

57 Among the several threats to the rock art heritage, resuspension and mobilization of
58 pigments (mostly ochres and charcoal) by cave water, including seepage and
59 condensation waters, are major hazards. Water films and drops can accumulate in
60 some parts of the cave walls and ceilings. Identifying the source of water
61 (condensation vs. infiltration) is crucial to develop protocols devoted to minimize the
62 impact on the cave features, including rock art and speleothems (Dublyansky and
63 Dublyansky, 2000; Fernández-Cortés et al., 2006).

64 The largest intakes of external water vapor in Altamira Cave may occur during the
65 cave ventilation period (June to October) (Quindós et al., 1987; Cuezva et al., 2009;
66 García-Antón et al., 2013; Gázquez et al., 2016b; Sainz et al., 2017), when relatively
67 warm and moist air masses enter the cave and cool, forcing condensation. In order to
68 reduce the inputs of airborne particles (i.e. organic matter, fungi and bacteria) that
69 could deteriorate the Paleolithic rock art of Altamira Cave, an artificial metal door was
70 installed in 2008 between the *Entrance Hall* (~20 m apart from the entrance) and the
71 rest of the cave. This intervention has had a positive impact on the microclimate
72 stability of the inner cave sectors in terms of temperature stability and decrease in
73 airborne particles (Sainz et al., 2018); however, the role of this artificial barrier in the

condensation processes in the cave has not been investigated to date. Indeed, specific studies on water condensation in Altamira Cave have not been performed yet.

Direct measurements of the condensation/evaporation processes have been conducted previously in caves worldwide by using suspended glass plates (Sarbu and Lascu, 1997), lysimeters and metallic devices (Dublyansky and Dublyansky, 1998; Gázquez et al., 2015a; 2017b) and refrigerated containers (Tarhule-Lips and Ford, 1998; Liñán et al., 2021), in order to quantify the magnitude of these mechanisms. Electrical devices coupled to data loggers have been utilized also to quantify condensation in caves (De Freitas and Schmekal, 2006). In addition, indirect measurements of the effects of condensation have been conducted by monitoring weight loss of rock tablets (Calaforra, 1996; Klimchouk et al., 1996; Tarhule-Lips and Ford, 1998; Klimchouk and Aksem, 2002; White et al., 2021), using micro-erosion meter measurements of cave surface retreatment (Calaforra and Forti, 1993; Klimchouk et al., 1996; Gázquez et al., 2015a) and determining thickness and age of weathering rinds (Auler and Smart, 2004). Indirect estimates of condensation/evaporation can be also obtained from microclimate monitoring of cave atmosphere and rock temperatures (De Freitas et al., 2003; Fernández-Cortés et al., 2006). Furthermore, theoretical approaches to the condensation mechanisms in caves have been developed in the last decades (Dreybrodt et al., 2005; Gabrovšek et al., 2010). More recently, thermal image analyses have been used to quantify condensation-evaporation processes in caves (Liñán et al., 2021).

The oxygen and hydrogen isotopes composition of water [$^{18}O/^{16}O$ and $^{2}H/^{1}H$ or $\delta^{18}O$ and δD, respectively, when standardized to the international water standard Vienna-Standard Mean Ocean Water (V-SMOW)] has been widely used to track a variety of processes in the hydrosphere (Bowen et al., 2019 and references therein), including

recent preliminary studies of condensation water in caves by Liñán et al. (2021). These authors found that condensation waters in Nerja Cave, southern Spain, display higher $\delta^{18}O$ and δD values and lower d-excess values during the cave ventilation periods than during the rest of the year. This seasonal pattern was attributed to the impact of evaporation on condensation water, which takes place during the cave ventilation period because of low relative humidity in the cave atmosphere (60-80%).

In addition to the traditional measurements of $\delta^{18}O$ and δD in waters, recent analytical advances have permitted obtaining precise measurements of the triple oxygen isotope composition ($\delta^{17}O$ and $\delta^{18}O$) (Barkan and Luz, 2005; Steig et al., 2014). The $\delta^{17}O$ deviations with respect to the $\delta^{17}O$–$\delta^{18}O$ Global Meteoric Water Line (GMWL), which has a proposed slope of 0.528, are expressed as ^{17}O-excess [$^{17}O\text{-excess} = \ln(\delta^{17}O/1000 + 1) - 0.528 \ln(\delta^{18}O/1000 + 1)$] (Barkan and Luz, 2005; Luz and Barkan, 2010). This reference slope is commonly used to express triple oxygen deviation in the hydrological cycle (Aron et al., 2021; Surma et al., 2021).

The ^{17}O-excess parameter in rainfall has been found to be sensitive to variations in relative humidity at the moisture source, with smaller temperature dependence than d-excess (d-excess=$\delta D - 8 * \delta^{18}O$) (Barkan and Luz, 2005, 2007; Luz and Barkan, 2010; Uechi and Uemura, 2019). Likewise, other parameters, including raindrop re-evaporation and moisture recycling during water vapor transport can modulates the final ^{17}O-excess signal of rainwater (Tian et al., 2018; Giménez et al., 2021). Thus, measuring the triple oxygen and hydrogen isotope composition of water can help to track environmental conditions (e.g. temperature vs. relative humidity) during water phase changes and during transport of water vapor masses (Aron et al., 2021; Surma et al., 2021).

Here, we conducted a 7-years monitoring study of stable isotopes ($\delta^{17}O$, $\delta^{18}O$, $\delta^{2}H$ and derived parameters d-excess and ^{17}O-excess) in condensation water and dripwater in Altamira Cave. We aim to identify isotopic differences between seepage and condensation water, in order to assess whether the numerous droplets observed in the ceiling of the *Polychrome Hall* of Altamira Cave are associated with either condensation or infiltration water. In addition, we investigate the origin of vapor for water condensation and the spatiotemporal pattern of the condensation mechanisms in this cave. To this end, we analyzed waters deposited on artificial supports in several locations of the cavity, as well as dripwater from fast drips (i.e. discharge point related to seepage of meteoric water) and ceiling droplets with no apparent dripping (presumably associated with water condensation) in the *Polychrome Hall*. The microclimate characteristics related to cave atmosphere ventilation (air temperature, relative humidity and CO_2 content) were monitored during the length of the study, in order to characterize the parameters that control the cave ventilation pattern and to identify connections with the condensation processes. We use an isotopic mixing model to demonstrate that different sources of water vapor contribute to condensation water in Altamira Cave and that the relevance of these sources change temporally and spatially.

2. Setting and cave description

Altamira Cave (43º22'37''N; 4º07'11''W) is located near the village of Santillana del Mar (Cantabria, northern Spain), at an elevation of 152 m a.s.l and 4.5 km from the Cantabrian Sea. The cavern runs NW-SE and has developed along a subhorizontal sequence of Cenomanian-Turonian marine carbonates (Hoyos *et al.*, 1981) where the

147 difference in level between the entrance and its deepest part (*Grave Hall*) is barely 26
148 m. Several cave sections can be distinguished according to their morphology and
149 distance/depth from the entrance: the *Entrance Hall* is a ~20 m-long horizontal hall;
150 from there, access to the rest of the cave is via an artificial door located in a narrow
151 passage, ~2 m wide. Beyond, the cave divides along two branches. To the east is the
152 *Polychrome Hall*, ~15 m long, ~7 m wide and up to 3 m high and lying about 2 m lower
153 than the cave entrance. The other branch gives access to *Walls Hall*, roughly 50 m in
154 length, 20 m wide and up to 7 m high; located ~6 m below the entrance.

155 A passage, roughly 60 m long runs SE-NE into the *Great Hall*. From here, artificial
156 stairs carved in the rock lead to *Grave Hall*, lying ~15 m below the cave entrance and
157 containing an ephemeral water pool that only appears during periods of high dripwater
158 discharge. To the South, along a 10 m-long passage, lies the *Shower Hall*. This in turn
159 leads into the *Well Hall*, at the depth of 12 m beneath the cave entrance. Finally, there
160 is a meandriform sub-horizontal passage (called the *Horsetail*) approximately 40 m
161 long that represents the innermost cave area. The thickness of the cap rock overlaying
162 the cave varies from 2 to 18 m (Elez *et al.*, 2013) (Fig. 1). There is no permanent
163 running watercourse inside the cave.

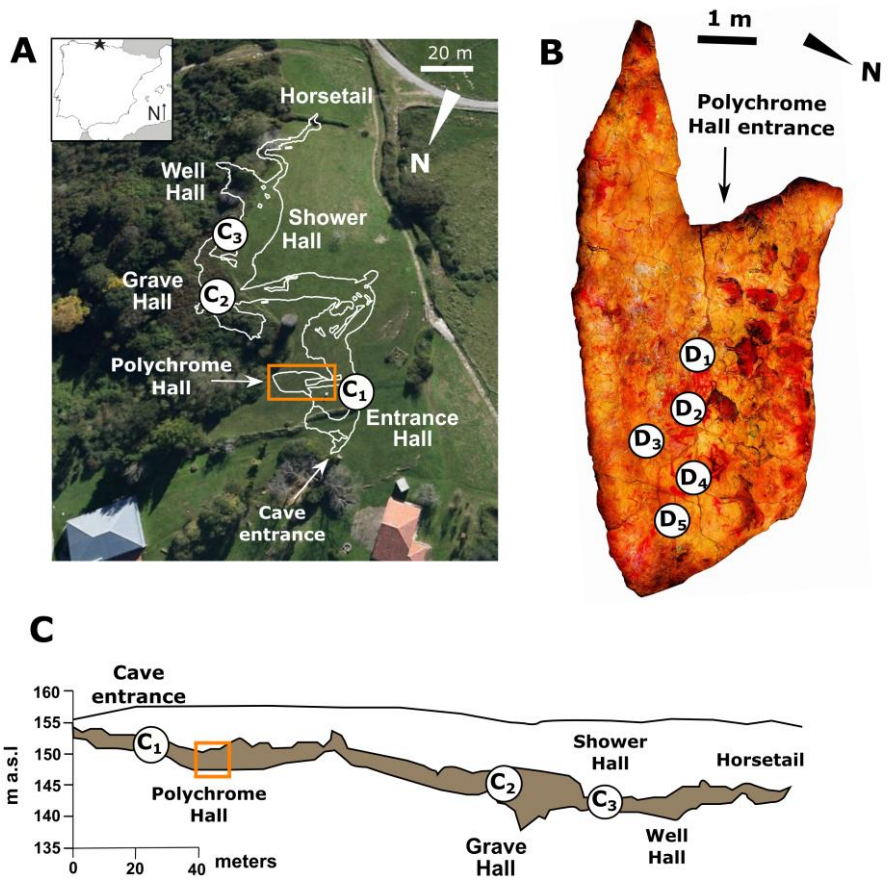

164

165 **Figure 1. A.** Location of Altamira Cave and distribution of the sampling sites in the
166 cavity, including artificial supports to collect condensation water (C1, C2 and C3); B.
167 View of the ceiling of Polychrome Hall (location is marked in orange rectangles in
168 panels 1A and 1C) with collection locations for the natural dripwater (D1) and droplets
169 (D2-D5) labelled; C. Vertical profile of Altamira Cave and location of the sampling sites
170 (modified from García-Antón et al., 2014).

171

172 The climate in this region is Oceanic (Cfb climate type, according to the Köppen
173 climate classification). The rainfall is generally abundant, exceeding 1,000 mm/year.
174 July is the driest month (30 mm on average) and the rainiest period occurs from
175 October to December (Fig. 2). The mean external air temperatures are minimum in

January (9 °C) and maximum in July (21 °C). The vegetation coverage over the cave is dominated by grasses with minor presence of scrubs and trees (Fig. 1A).

Altamira Cave has a relatively stable microclimate, with air temperatures that vary less than 2 ^{o}C throughout the year in the innermost areas (*Well Hall* and *Horsetail*) and up to 5 ^{o}C in the outermost part of the cave (*Entrance Hall*) (Gázquez et al., 2016). The mean temperature in the *Polychrome Hall* during the period of study was 14.2±0.5 ^{o}C (maximum value of 15 ^{o}C and minimum value of 13.2 ^{o}C).

The air temperature and ventilation regime of Altamira Cave are fundamentally controlled by the annual thermal oscillations of the outside air temperature and the water saturation of the epikarst and the soil over the cave (Cuezva et al., 2011). The outside temperature oscillations are transmitted into the cave through the rock, which attenuates its amplitude and causes a lag between the outer thermal wave and the temperature of the subterranean atmosphere (Elez et al., 2013). Consequently, the cave ventilation period occurs in summer (June to October), while the cave stagnation period takes place in winter (November to May). The annual variation of in-cave air temperature exhibits a sinusoidal pattern with a thermal lag time (~2 months on average) between the innermost and outermost cave areas that depends on the outside temperature and the thickness of the rock over the different cave sectors (Quindós et al., 1987; Cuezva et al., 2011; Sainz et al 2017).

3. Methods

We assess the spatial gradient and temporal variability of the isotopic composition of condensation water and dripwater, as well as cave environmental parameters (air temperature, relative humidity and CO_2 content) in Altamira Cave, by monitoring and

repeatedly sampling from the cave entrance to more stable locations deeper within the cave.

3.1. Water sampling

From November 2014 to March 2017, condensation water that accumulates on a metallic door that separates the Entrance Hall and the rest of the cave (site C1 in Fig. 1) was collected using disposable pipets (~200 μl) (n=11). From March 2017 to October 2020, sampling was conducted approximately every two weeks in the same location, but condensation was collected from the metal support of a thermometer that is 1 m apart from the door. In addition, condensation water from two inner cave locations (sites C2 and C3 in Fig. 1) was collected from metal supports of thermometers using the same method from March 2017 to August 2020. Water samples were stored at 4 ^{o}C in 2 ml glass tubes provided with a micro-insert (~300 μl; Thermo Fisher, n. 10376102) and capped with silicone septum caps. A total of 76 surveys were conducted and a total of 192 condensation water samples from artificial supports were collected.

Dripwater samples from a relatively fast discharge point (maximum of 143 ml/day; mean of 61±21 ml/day) in the *Polychrome Hall* (site D1 in Fig. 1) were collected approximately every two weeks between March 2017 and August 2020. A graduated container was placed under the drip point and volumes were recorded between surveys in order to calculate drip rates. Water samples were collected from this container and stored in 14 ml glass tubes at 4 ^{o}C. A total of 76 dripwater samples were collected from site D1. In addition, water droplets from four selected locations of the ceiling of the *Polychrome Hall* (i.e., sites with no visibly dripping; D2-D5 in Fig. 1) were collected and stored using the same protocol as for condensation water. A total of 254

samples from these four locations were taken every two weeks between March 2017 and October 2020.

3.2. Stable isotopes analysis

Samples collected between July 2013 and July 2014 were analyzed for $\delta^{18}O$ and δD using a L1102-i Picarro water isotope analyzer at the Godwin Laboratory for Paleoclimate Research, University of Cambridge, UK. Samples collected between August 2014 and October 2020 were analyzed for $\delta^{17}O$, $\delta^{18}O$ and δD at the Laboratory of Stable Isotopes of the University of Almeria, Spain using a L2140-i Picarro water isotope analyzer (Picarro, Inc., Santa Clara, California, USA).

Each sample was injected ten times into the vaporizer (A0211 manufactured by Picarro, Inc.), which was heated to 110°C. Potential contamination produced by organic compounds in water, which may affect specially the measurements of ^{17}O-excess values, was removed by using a Picarro micro-combustion module (MCM) coupled to the L2140-i Picarro analyzer (Gázquez et al., 2015b). Memory effects from previous samples were avoided by rejecting the first three analyses. Values for the final 7 injections were averaged with a typical mean instrumental precision (±1SD) of ±0.02‰ for $\delta^{17}O$, ±0.03‰ for $\delta^{18}O$ and ±0.19‰ for δD when using the L2140-i Picarro analyzer, as observed from repeated analysis of an in-house water standard (n=54) together with the water samples. The instrumental precision of the L1102-i Picarro analyzer was ±0.05‰ for $\delta^{18}O$ and ±0.6‰ for δD. The in-run drift of the instruments was monitored by analyzing a water standard (BOTTY) every 6 samples. The results were normalized against V-SMOW-SLAP in the case of triple oxygen isotopes, and against V-SMOW-SLAP-GISP in the case of hydrogen isotopes, by analyzing internal

248 standards before and after each set of fifteen to twenty samples (see Supplementary
249 Table 1 for examples of our calibration). To this end, three internal water standards
250 (JRW, $\delta^{17}O$=-9.99‰, $\delta^{18}O$=-18.90‰ and δD=-146.5‰; BOTTY, $\delta^{17}O$=-3.88‰, $\delta^{18}O$=-
251 7.40‰ and δD=-50.38‰; SPIT, $\delta^{17}O$=-0.09‰, $\delta^{18}O$=-0.15‰ and δD=-0.44‰) were
252 calibrated previously for triple oxygen isotopes against V-SMOW and SLAP by a two-
253 points calibration, using $\delta^{17}O$ of 0.0‰ and -29.69865‰, respectively, and $\delta^{18}O$ of 0.0‰
254 and -55.5‰, respectively (Schoenemann et al., 2013). This approach assumes V-
255 SMOW and SLAP have ^{17}O-excess= 0. The δD of the internal standards was calibrated
256 against V-SMOW, GISP and SLAP using a three-points calibration. Note that GISP
257 does not have an accepted $\delta^{17}O$ value, so cannot be used for triple oxygen isotope
258 calibration. Instead, the GISP water standard was analyzed as an unknown during the
259 calibration of our internal standards, yielding an average ^{17}O-excess value of 19±18
260 per meg. This value is in good agreement with the results reported by previous studies
261 (e.g. Schoenemann et al. 2013; 22±11 per meg).

262 The ^{17}O-excess was calculated for each injection using the normalized $\delta^{17}O$ and $\delta^{18}O$
263 values. The final reported value is the average of ^{17}O-excess values from all 7 suitable
264 injections. All ^{17}O-excess values are given in per meg units (1 per meg = 0.001‰).
265 Typical in-sample ^{17}O-excess and d-excess precisions (1SD) in water standards
266 (BOTTY, n=54), were 13 per meg and 0.2‰, respectively, similar to the precision
267 obtained by other CRDS instruments (Wassermann et al., 2021).

268

269 **3.3. Microclimate monitoring**

270 Measurements of air temperature and air CO_2 concentrations were conducted at sites
271 C1, C2 and C3, in the *Polychrome Hall* (Fig. 1) and outside the cave close to the

entrance door, between January 2014 and October 2020. Rainfall amount was recorded by a meteorological station located in the terrain over the cave during the length of the study. A total of 191 monitoring campaigns were conducted during this period, typically every two weeks and between 10 a.m. and 12 p.m. The in-cave temperature measurements used mercury thermometers with a precision of ±0.05 ^{o}C that were installed in the cave at the beginning of this study. For the measurements of the external air we used a portable digital temperature probe (Vaisala HMP155) with a precision of ±0.1 ^{o}C. The concentration of CO_2 in air was analyzed in situ using a Testo 445 (mod. 0560-4450) device with a precision of 5%. Relative humidity was measured using EE21 Series instrument, with an accuracy of ±3%. Additionally, the automatic measurements performed by this device have being reproduced with grab sampling measurements carried out with an aspiration psicrometer Lambrecht kG Göttingen (model 761), with a resolution of 2%.

3.4. Stable isotope modeling

We modeled the stable isotope composition of condensation water at site C1 by using a two-endmember mixing model, in which the endmembers are the water vapor generated within the cave (autochthonous water vapor hereafter) and the water vapor that enters the cave from outside during the cave ventilation period (allochthonous water vapor hereafter) (see Supplementary Table 2 for model parametrization and calculations). The CO_2 content in air is assumed to reflect the degree of atmosphere ventilation at site C1. This means that the maximum CO_2 content recorded at site C1 during the cave stagnation period (5525 ppm) represents 0% ventilation and the outside CO_2 content during the length of this study (470 ppm) represents 100% ventilation. We assume a linear relationship between the CO_2 content and the degree

297 of cave ventilation at site C1. The isotopic composition of the two water vapor
298 reservoirs can be approximated by assuming equilibrium conditions with
299 environmental water (i.e. cave water and meteoric water). We use the mean isotopic
300 composition of dripwater at site D1 to represent the isotopic composition of cave water
301 ($\delta^{18}O$ = -5.9±0.1‰, δD= -32.8±0.4‰, d-excess= 14.4±0.6‰, ^{17}O-excess = 25±7 per
302 meg, during the length of this study). We use the long-term (i.e. 15 years mean)
303 monthly values of $\delta^{18}O$ and δD in rainfall recorded by the meteorological station of
304 Santander city, 15 km apart from Altamira Cave (data from the Global Network of
305 Isotopes in Precipitation of the International Atomic Energy Agency, period 2000-2015;
306 IAEA/WMO 2021) to calculate the isotopic composition of the external vapor. Because
307 there is no $\delta^{17}O$ data, and therefore ^{17}O-excess cannot be calculated for precipitation
308 near Altamira Cave, we assume that the ^{17}O-excess in rainfall correlates linearly with
309 $\delta^{18}O$, as reported by Giménez et al. (2021) in the Pyrenees (northern Spain), ~220 km
310 from Altamira Cave. These authors found that the $\delta^{18}O$-^{17}O-excess relationship has a
311 slope of 3.8 per meg/‰ at this site. Then, we use this relationship to calculate the ^{17}O-
312 excess of rainfall in the setting of Altamira Cave from the $\delta^{18}O$ of rainfall. Finally, the
313 $\delta^{17}O$ is calculated from $\delta^{18}O$ and ^{17}O-excess.
314 The isotopic compositions of both, the autochthonous and the allochthonous water
315 vapor are controlled by the in-cave and external temperatures, respectively.
316 Equilibrium liquid-vapor fractionation factors for $\delta^{18}O$ ($\alpha^{18}O_{eq}$) and δD (αD_{eq}) are
317 calculated here as a function of temperature using the equations of Horita and
318 Wesolowski (1994). The $\alpha^{17}O_{eq}$ is calculated as $\alpha^{17}O_{eq} = \alpha^{18}O_{eq}{}^{\theta}$, where θ is
319 0.529±0.001 (Barkan and Luz, 2005).
320

4. Results

A total of 481 water samples from Altamira Cave were analyzed for triple oxygen and hydrogen isotopes. The summary of the $\delta^{17}O$, $\delta^{18}O$, δD values and derived parameters d-excess and ^{17}O-excess are given in Table 1 and Supplementary Table 3. The results are plotted with time in Figure 2, along with the monitored climate parameters at site C1.

4.1. Condensation water from artificial supports

4.1.1. Outmost cave sector (site C1)

The $\delta^{18}O$ and δD values of condensation water from the outmost part of the cave correlate linearly ($\delta D = 6.9(\pm0.2)*\delta^{18}O + 9.1(\pm1.1)$; $R^2=0.94$, p-value<0.05). The slope of this relationship is similar to that of the Local Meteoric Water Line ($\delta D = 7.1(\pm0.1)*\delta^{18}O + 7.4(\pm0.8)$; $R^2=0.93$, p-value<0.05) in Santander city (15 km from Altamira Cave; IAEA/WMO, 2021), while the intercept is slightly higher than that of the LMWL (Fig. 3A). The d-excess and ^{17}O-excess values of condensation water at site C1 are not correlated with $\delta^{18}O$ ($R^2=0.1$, p-value>0.05) (Fig. 3). The $\delta^{18}O$ and δD values are higher during the cave ventilation period (-4.6±0.7‰ and -22.4±4.6‰, respectively), while during the rest of the year are lower and less variable (-5.6±0.4‰ and -30.0±3.0‰, respectively) (Fig. 2 and 4). The ^{17}O-excess values of condensation water at site C1 average 27±11 per meg and ranges from 6 to 60 per meg. No systematic differences in this parameter have been between the ventilation period (27±12 per meg) and the stagnation period (28±9 per meg), probably due to insufficient analytical precision of the measurements (±13 per meg, 1SD) (Fig. 4). The d-excess

shows more variable values during the ventilation period (14.3±2.1‰) than during the cave stagnation period (15.2±1.1‰) (Fig. 2 and 4).

4.1.2. Inner cave sectors (sites C2 and C3)

The mean $\delta^{18}O$ and δD values of condensation water from the two sites investigated in the inner part of the cave (sites C2 and C3) are indistinguishable within errors (Table 1 and Supplementary Table 3). The $\delta^{18}O$ and δD values correlate linearly ($\delta D = 4.5(\pm0.4)*\delta^{18}O - 6.0(\pm1.4)$; $R^2=0.76$, p-value<0.05) (Fig. 3). The annual variability is less than 0.3‰ (1SD) for $\delta^{18}O$ and less than 1.6‰ for δD and does not correlate with seasonal changes in the monitored air parameters (temperature and CO_2 concentration) in the cave (Fig. 2). Indeed, no significant differences in all the measured isotopic parameters can be distinguished between the cave ventilation period and the stagnation period (Table 1 and Fig. 4). The correlation between d-excess and $\delta^{18}O$ is negative and statistically significant ($R^2=0.63$, p-value<0.05) (Fig. 3). There are no significant correlations between ^{17}O-excess and $\delta^{18}O$ ($R^2=0.01$, p-value>0.05) or between ^{17}O-excess and d-excess ($R^2=0.12$, p-value>0.05) (Fig. 3).

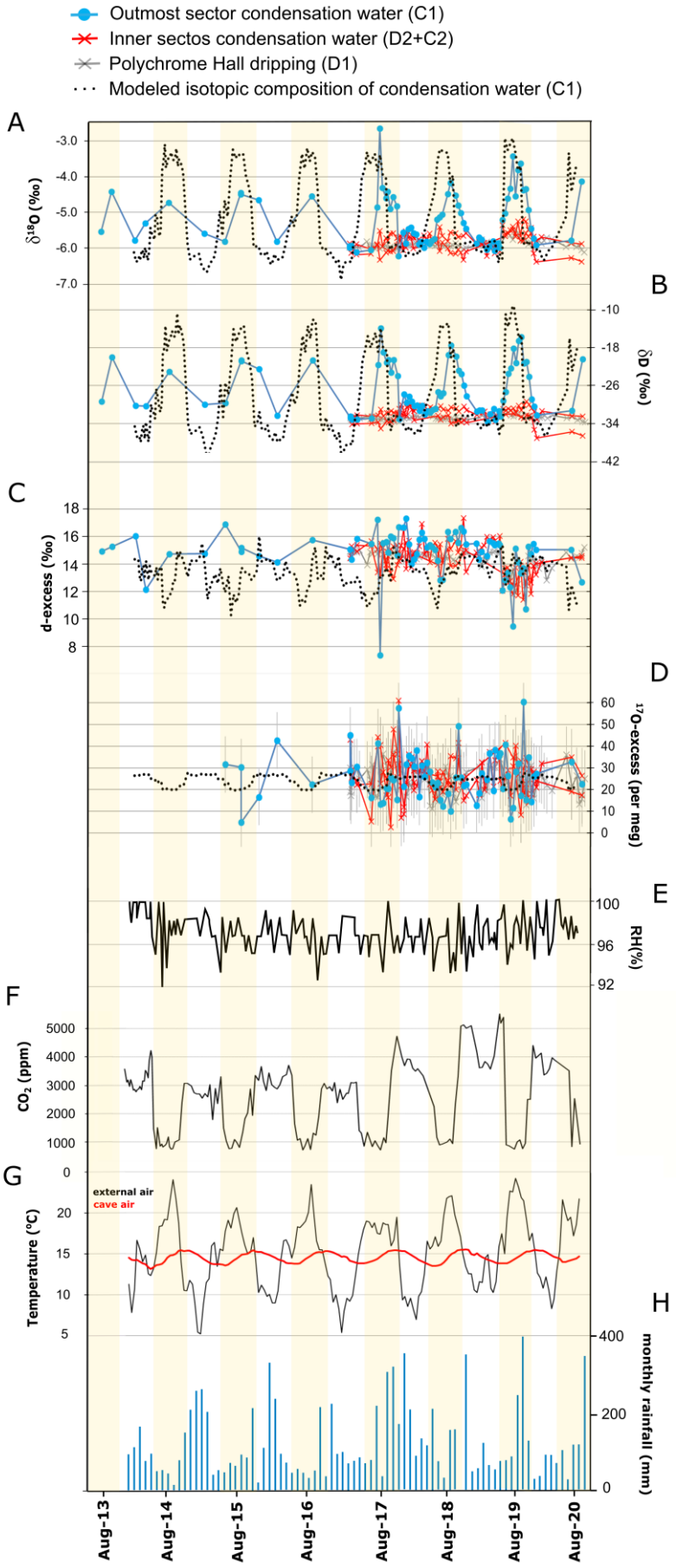
Outmost sector condensation water (C1)
Inner sectos condensation water (D2+C2)
Polychrome Hall dripping (D1)
Modeled isotopic composition of condensation water (C1)
A
δ18O (‰)
B
δD (‰)
C
d-excess (‰)
D
17O-excess (per meg)
E
RH(%)
F
CO2 (ppm)
G
Temperature (°C)
external air
cave air
H
monthly rainfall (mm)
Aug-13
Aug-14
Aug-15
Aug-16
Aug-17
Aug-18
Aug-19
Aug-20

360

Figure 2. Temporal variations of oxygen and hydrogen stable isotopes (A. $\delta^{18}O$; B. δD; C. d-excess; D. ^{17}O-excess) of condensation water and dripwater Altamira Cave (site C1 in Fig. 1). Results of modeled isotope composition of condensation water at site C1 are displayed (dashed lines). Relative humidity (E) (site C1), CO_2 concentration in the cave atmosphere (F) (site C1), air temperature in the cave (site C1) and outside (G) and monthly rainfall in Santillana del Mar (H) are presented. A 2-point moving average has been used to represent air temperature. The yellow bands represent cave ventilation periods (June to October).

4.2. Dripwater (site D1) and ceiling droplets (sites D2, D3, D4 and D5) in the *Polychrome Hall*

The $\delta^{18}O$ of the fast discharge point in the *Polychrome Hall* (site D1) ranged from -6.1 to -5.5‰, with a mean of -5.9±0.1‰. The δD ranged from -33.7 to -31.6‰, with a mean of -32.8±0.4‰. The d-excess varied between 11.9 and 15.0‰, with a mean of 14.4±0.6‰, and the ^{17}O-excess varied between 11 and 39 per meg with a mean of 25±7 per meg (Table 1). No clear systematic seasonal patterns have been observed in the isotopic parameters during the 4-years monitoring (Fig. 2 and 4).

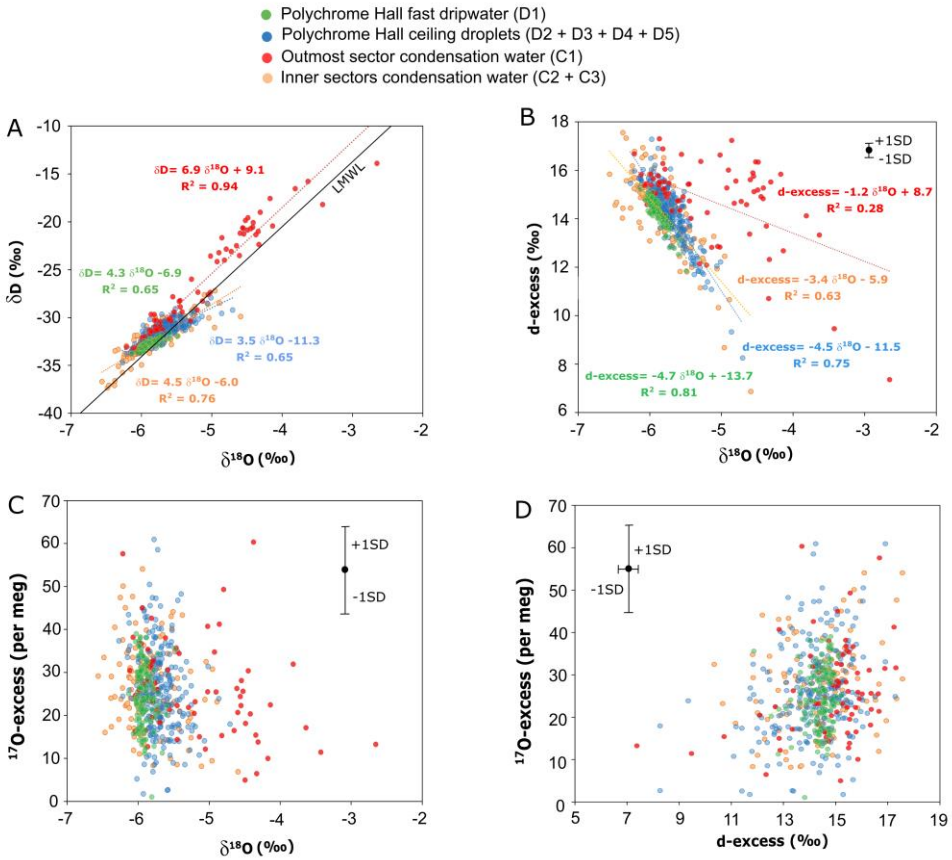

Figure 3. Cross-plot of isotopic parameters (A. δD vs. $\delta^{18}O$; B. d-excess vs. $\delta^{18}O$; C. ^{17}O-excess vs. $\delta^{18}O$; D. ^{17}O-excess vs. d-excess) in condensation waters (sites C1, C2 and C3), dripwater (D1) and ceiling droplets with no apparent dripping in the ceiling of the *Polychrome Hall* (D2, D3, D4 and D5) of Altamira Cave. The local meteoric water line (LMWL; IAEA/WMO, 2021) is given for comparison in panel A. The errors for $\delta^{18}O$ and δD are smaller than the symbols. The mean analytical errors for d-excess (0.2‰) and ^{17}O-excess (13 per meg) are represented in panels B, C and D.

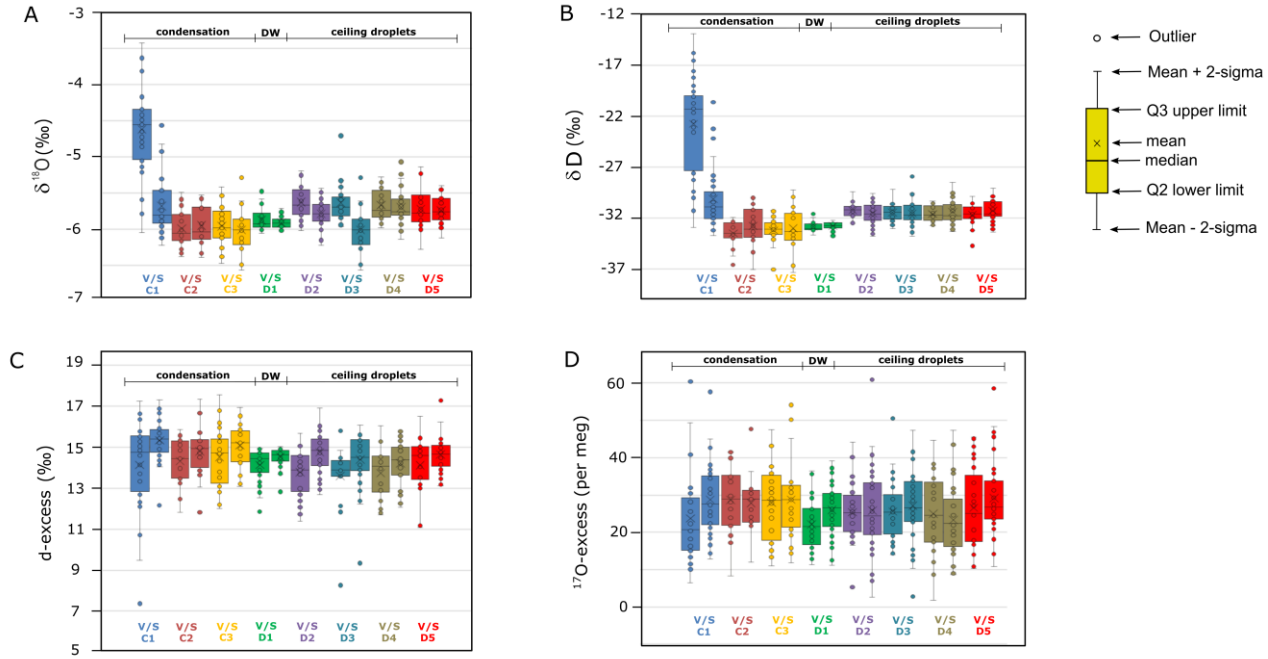

386

387 **Figure 4.** Box and whisker plots of $\delta^{18}O$ (A), δD (B), d-excess (C) and ^{17}O-excess
388 (D) of condensation water in the outmost cave sector (sites C1) and in the inner
389 sectors (sites C2 and C3), as well as dripwater (DW, site D1) and ceiling droplets
390 with no apparent dripping (sites D2, D3, D4 and D5) in the *Polychrome Hall* of
391 Altamira Cave. Results of the cave ventilation period (V; June to October) and the
392 stagnation period (S; November to May) are displayed for comparison.

393

394 The isotopic composition of the ceiling droplets with no apparent dripping in the
395 *Polychrome Hall* (D2, D3, D4, D5) are statistically indistinguishable (Table 1 and Fig.
396 4). Taking altogether, the $\delta^{18}O$ of the ceiling droplets ranged from -6.3 to -4.7‰, with
397 a mean of -5.7±0.2‰. The δD ranged from -34.7 to -27.9‰, with a mean of -31.4±1‰.
398 The d-excess varied between 8.0 and 17.3‰, with a mean of 14.2±1.3‰, and the ^{17}O-
399 excess did between 2 and 61 per meg with a mean of 26±10 per meg. No systematic
400 seasonal patterns have been observed in the isotopic parameters during the 4-years

401 monitoring (Table 1 and Fig. 4). The $\delta^{18}O$ and δD in the four points showed similar
402 patterns with time (R^2>0.4 and p-value<0.05).

403

404 **4.3. Microclimate parameters**

405 The air temperature in the *Entrance Hall* (site C1 in Fig. 1) ranged from 13.1 from 15.7
406 ºC, with a mean value of 14.5±0.6 ºC. Maximum temperatures were recorded in
407 September and minimum temperatures correspond to March. In the *Polychrome Hall*
408 (sites D1, D2, D3, D4 and D5 in Fig. 1) air temperature oscillated between 13.2 and
409 15.0 ºC and the mean value was 14.2±0.5 ºC. Maximum temperatures were recorded
410 in December, while minimum temperatures correspond to June. The temperature in
411 the innermost sector of the cave (locations C2 and C3 in Fig. 1) varied between 12.5
412 and 14.5 ºC, with a mean of 13.7±0.2 ºC. Maximum temperatures were recorded
413 between October and February and minimum temperatures corresponded to June and
414 July. The temperature outside measured during the visits to the cave (between 10 a.m.
415 and 12 p.m) ranged from 2.9 to 25.1 ºC, with a mean of 15.1±4.7 ºC. Maximum
416 temperatures outside were recorded in August, while minimum temperatures
417 correspond to January and February. August and July are the driest month of the
418 series, while the autumn and spring months concentrate most of the annual
419 precipitation (Fig. 2).

420 The mean CO_2 in the *Polychrome Hall* was 2580±1423 ppm, with lower values around
421 1000 ppm from June to October ("ventilation period") and higher values around 3000
422 ppm were recorded between November and May ("stagnation period"). At site C1, the
423 CO_2 content varied between 724 and 5525 ppm. The change from lower to higher CO_2

conditions (and vice versa) generally takes place in around 2 weeks, mainly depending on the external meteorology.

Relative humidity (RH) in the *Polychrome Hall* was 96.8±1.9% on average and ranged from 92% to 100%. In the outmost part of the cave (site C1), RH ranged from 88% to 100% and averaged 96.5±2.3% (Fig. 3E). Generally, the lowest RH values correspond to the cave ventilation period and values closer to 100% are characteristic of the stagnation period. The RH in the inner cave sector is slightly higher and closer to saturation (>97%), with no significant seasonal changes (Gázquez et al., 2016; Sainz et al., 2018).

4.4. Results of isotope modeling

The modeled $\delta^{18}O$ and δD values of condensation water for the sectors near the cave entrance (site C1) show a seasonal pattern, with higher values (up to -2.9‰ and -8.4‰, respectively) during the cave ventilation period and lower values during the stagnation period (down to -6.9‰ and -43.7‰, respectively) (Fig. 1). The modeled d-excess values of condensation water ranges from 10.1 to 16.2 ‰, with the lowest values corresponding to the ventilation period and higher values are obtained for the stagnation period. We found that the expected range of ^{17}O-excess in condensation water is only of 9 per meg. Note that this variability is smaller than the analytical precision of our ^{17}O-excess measurements (~13 per meg). The highest ^{17}O-excess values occur during the cave stagnation period (maximum value of 28 per meg) and lower values are observed during the cave ventilation period (minimum of 19 per meg).

We tested the sensibility of the isotopic composition of condensation water to the different parameters consider by our model (external air temperature and cave atmosphere temperature, the isotopic composition of cave dripwater and meteoric

448 water and the degree of cave atmosphere ventilation). As expected, we found that
449 during the cave stagnation period the isotopic composition of condensation water at
450 site C1 is insensitive to changes in the outside air temperature and variations in the
451 isotopic composition of meteoric water (Supplementary Fig. 1 and 3). Also, changes
452 in the cave atmosphere temperature during the stagnation period have an insignificant
453 impact on the isotopic composition of condensation water (Supplementary Fig. 2),
454 given the small temperature variations in the cave atmosphere temperature (<5 ^{o}C).
455 In contrast, the isotopic composition of condensation water at site C1 during the cave
456 ventilation period is relatively sensitive to the changes in the external air temperature
457 (e.g. 1‰ δ^{18}O increase for each increment of 10 ^{o}C) (Supplementary Fig. 1). We found
458 that the δ^{18}O and δD values of condensation increase linearly with the δ^{18}O and δD
459 values of the external meteoric water (Supplementary Fig. 3), while changes in the
460 cave temperature atmosphere have little impact on the δ^{18}O and δD values of
461 condensation water (e.g. 0.2‰ δ^{18}O increase for an increment of 2 ^{o}C)
462 (Supplementary Fig. 2). Likewise, the secondary parameters d-excess and ^{17}O-excess
463 are insensitive to change in the external parameters during the cave stagnation period
464 (Supplementary Figures 1 to 3). In contrast, during the ventilation period, the d-excess
465 of condensation water in the outmost cave sectors is significantly impacted by changes
466 the external air temperature (i.e. 3.7‰ d-excess increase for each increment of 10 ^{o}C)
467 and by changes in the d-excess of meteoric water. The modeled ^{17}O-excess values of
468 condensation water at site C1 during the ventilation period are barely affected by
469 changes in the internal and external air temperatures (i.e. 1 per meg increase for each
470 increment of 10 ^{o}C).
471

5. Discussion

The difference in isotopic composition of two water reservoirs (e.g. liquid and vapor) in equilibrium during phase change depends mostly on temperature that controls the equilibrium isotope fractionation factors between the two phases (e.g. $\alpha^{18}O_{water\text{-}vapor}$ and $\alpha D_{water\text{-}vapor}$) (Craig et al., 1963; Horita and Wesolowski, 1994). Additionally, when the evaporation-condensation process occurs under RH<100%, kinetic isotope fractionation can take place, which magnitude depends mostly on relative humidity and the degree of turbulence on the liquid-vapor boundary layer (i.e. wind) (Cappa et al., 2003; Landais et al., 2006; Barkan and Luz, 2007, Luz et al., 2009). In caves, relative humidity is close to 100% (e.g. Fig. 2) and wind speed is generally insignificant compared to outside (Gázquez et al., 2016); thus, equilibrium isotope process is expected to prevail over kinetic isotope fractionation during phase changes. Consequently, for the particular case of condensation in caves, the most important parameters controlling the isotopic composition of condensation water are temperature and the isotopic composition of water vapor.

Our monitoring data show that Altamira Cave directly, and rapidly, exchanges gases with the external atmosphere during the cave ventilation period (June to October), when intakes of water vapor from outside are expected. Note that the seasonal environmental changes outside are considerably larger than in the cave. This includes larger temperature changes and varying isotopic of compositions of water vapor. Indeed, the isotopic composition of summer rainfall in this region is more enriched (e.g. $\delta^{18}O$~-3.5‰ in June) than in winter (e.g. $\delta^{18}O$~-6.7‰ in January) (IAEA/WMO 2021) and external water vapor is assumed here to be in equilibrium with environmental liquid water outside. According to this, the isotopic composition of atmospheric vapor outside the cave during summer is expected to increase compared to winter

497 conditions. In contrast, the isotopic composition of the autochthonous water vapor
498 generated within the cave is expected to be less variable that outside because of cave
499 temperature is nearly constant and the vapor is in equilibrium with the cave dripwater,
500 which has almost constant isotopic values (Table 1 and Fig. 2). We evaluate the impact
501 of allochthonous water vapor entering the cave during the ventilation period on the
502 isotopic composition of condensation water at site C1 (*Entrance Hall*) by using a two-
503 endmember mixing model (Fig. 2 and Supplementary Table 2).

504 The magnitude and variability of the modeled isotopic values for site C1 agree with
505 our observations of $\delta^{18}O$ and δD of condensation water at site C1 (Fig. 2). Our model
506 demonstrates that the seasonal cycles recorded by the isotopic composition of
507 condensation water in the outmost part of the cave are a consequence of advection of
508 allochthonous water vapor from the external atmosphere. The "summer condensation
509 water" that accumulates during the ventilation period near the Entrance Hall is
510 isotopically enriched (i.e. higher $\delta^{18}O$ and δD values) compared to the "winter
511 condensation water" that derives from recycling of autochthonous water vapor
512 generated in the cave water during the stagnation period (Figs. 3 and 5). The relatively
513 constant $\delta^{18}O$ and δD values of autochthonous water vapor (ranges of 0.3‰ and 2.7‰,
514 respectively) is a consequence of the small cave temperature variability and the almost
515 constant isotopic values of seepage water through the seasonal cycle.

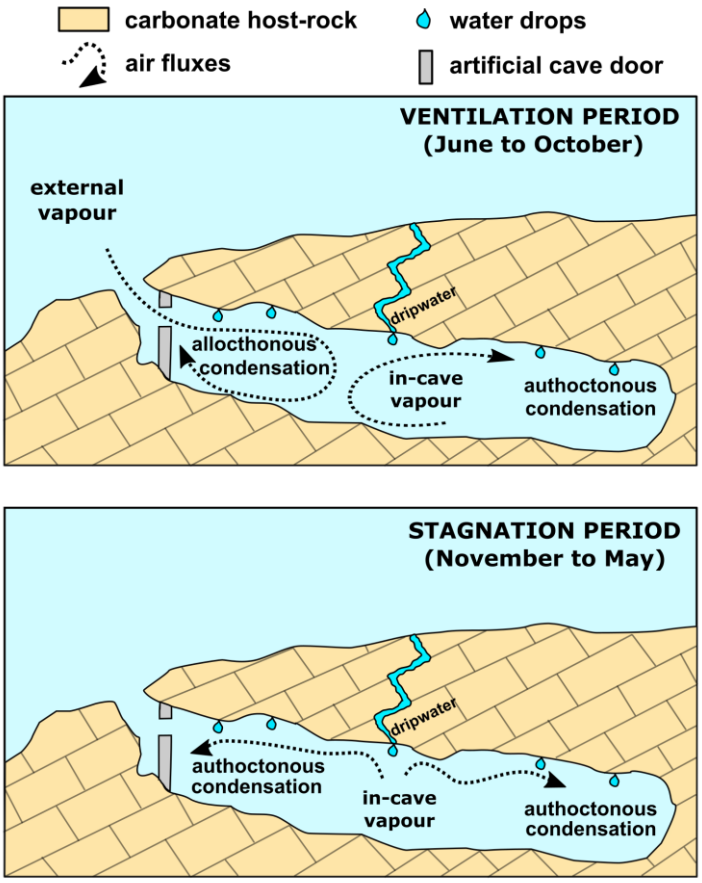

516

517 **Figure 5.** Conceptual diagram of condensation water systematic in Altamira Cave,
518 during the cave ventilation period (A) and the cave stagnation period (B). The inner
519 cave sectors are less affected by water vapor transported by air masses from outside
520 during the entire year, while the main source of vapor for condensation in these areas
521 is autochthonous water vapor generated from dripwater. The outmost areas receive
522 allochthonous water vapor from outside only during the ventilation period, while the
523 autochthonous vapor is the majority source of moisture for condensation in the entire
524 cave during the stagnation period. The metal door that separates the *Entrance Hall*
525 from the rest of the cave has been represented.

526

Condensation from allochthonous water vapor in caves seems to be analogue to recharge by “occult rain” detected in arid regions that occurs because of re-evaporation of local water and subsequent condensation of vapor on vegetation and soils (Aravena et al., 1989; Kaseke et al., 2017). If such vapor is re-condensed in any significant quantity before mixing with the larger tropospheric reservoir, the isotopic composition of the resulting condensation water will fall slightly above the LMWL (i.e. higher d-excess values), along a condensation line with a slope similar to the LMWL (Ingraham and Matthews, 1988, 1990; Clark and Fritz, 1997). Indeed, we found that y-intercept of the $\delta^{18}O$-δD correlation line of condensation water in the outmost part of the cave (site C1) is slightly higher (9.1±1.1‰) than that of the Local Meteoric Water Line (LMWL) (7.4±0.8‰), although their slopes are indistinguishable within errors (Fig. 3). Similarly, an offset between d-excess of condensation water and the LMWL has been observed in other caves (Gázquez et al., 2017b; Liñán et al., 2021).

Evaporation of condensation water can explain some of the d-excess outliers observed in the *Entrance Hall* that were recorded mostly during the cave ventilation period (e.g. three d-excess values ranging from 7 to 10.5‰ in summer 2017, 2018 and 2019; Fig. 4). These d-excess values are slightly lower than predicted by our model (Fig. 2C). Note that evaporated water normally show lower d-excess values (that correlates with $\delta^{18}O$ and δD) compared to non-evaporated waters (e.g. Luz et al., 2009; Gázquez et al., 2018; Voigt et al., 2021). However, the correlation between $\delta^{18}O$ and d-excess of condensation water in Altamira Cave is weak (R^2=0.28), the d-excess of condensation water remains generally high during the ventilation period (~15‰ and up to 17.3‰) and can occasionally show lower values during the rest of the year. In consequence, the seasonal variability of condensation water at site C1 cannot be

attributed to the effect of evaporation, but to the varying contributions of autochthonous and allocthonous water vapor.

The modeled ^{17}O-excess values of condensation water at site C1 vary from 19 per meg during the cave stagnation period to 28 per meg during the ventilation period (Fig. 2). No statistically significant seasonal trends in ^{17}O-excess of our analytical data have been observed in any of the sites investigated in this study, either in condensation water nor in dripwater. Recent studies showed that the δ^{18}O-^{17}O-excess relationship in rainwater in northern Spain (Villanua village, ~220 km from Altamira Cave) has a slope of 3.8 per meg/‰. Considering that the δ^{18}O of rainwater in Santander city varies seasonally by ~3‰, a range of ^{17}O-excess in rainwater of 12 per meg would expected. The expected ^{17}O-excess variability in dripwater of Altamira Cave is even smaller (2 per meg), considering the small δ^{18}O variability observed during the length of this study (0.5‰). Regarding that the mean reproducibility of our ^{17}O-excess measurements is 13 per meg (1SD), we conclude than the current analytical precision of the CRDS analyzers is insufficient to investigate the small ^{17}O-excess variability expected for condensation water and dripwater in caves.

As for condensation water in the inner cave sectors, the triple oxygen and hydrogen isotopic values in dripwater and its temporal variability (site D1) are indistinguishable from to those of condensation water collected from the inner cave sectors (sites C2 and C3). This suggests that water condensation from autochthonous water vapor in Altamira Cave cannot be differentiated from seepage water by using oxygen and hydrogen isotopes. Also, the isotopic composition of the ceiling droplets with no apparent dripping (sites D2, D3, D4 and D5) of the *Polychrome Hall* and the rest of condensation waters from the inner cave sectors (sites C2 and C3) show indistinguishable values within errors. No clear differences between the ventilation and

576 the stagnation periods has been identified. Thus, it is possible that the ceiling droplets
577 with of the *Polychrome Hall* are related to water condensation; however, contributions
578 of meteoric water infiltration and extremely slow drainage of the epikarst over this
579 chamber cannot be ruled out from our data.

580 We found that the small seasonal changes observed in the isotopic composition of
581 dripwater and condensation water in sectors relatively distant from the cave entrance
582 do not seem to be controlled by ventilation/stagnation regimen of the cave, since no
583 correlation with the CO_2 content or with in-cave air temperature has been observed
584 (Fig. 4). This indicates that the main source of vapor for condensation in these sites is
585 autochthonous water vapor from within the cave, with insignificant contributions of
586 allochthonous air masses, even during the ventilation period. This is probably related
587 to the fact that allochthonous water vapor condenses on cave surfaces closer to the
588 entrance and, likely on the artificial door that separates the *Entrance Hall* and the rest
589 of the cave, which is permanently closed. In consequence, the allochthonous water
590 vapor does not reach the inner cave sector even during the ventilation periods and
591 does not impact on the isotopic composition of condensation water in these areas.

592

593 **6. Conclusions**

594 We investigate the spatiotemporal variability of $\delta^{17}O$, $\delta^{18}O$, δD and derived ^{17}O-excess
595 and d-excess values of condensation water in Altamira Cave. Significant changes in
596 some of these parameters have been observed in the outmost cave sectors, while in
597 the inner/deeper cave parts the isotopic composition of condensation water is less
598 variable though the seasonal cycles. In particular, we found that the $\delta^{18}O$ and δD of
599 condensation water in the cave sectors closer to the entrance during the ventilation

600 period (June to October) are higher than during the stagnation period (November to
601 May). We evaluate the role of cave ventilation pattern in the condensation process in
602 this cave sector by using an isotope mixing model. We found that the isotopic
603 composition of condensation water near the cave entrance during the ventilation
604 period agrees with the expected values of water condensed from allochthonous water
605 vapor, while the prevailing mechanism during the stagnation period is condensation
606 from autochthonous water vapor generated within the cave.

607 Importantly, no significant differences have been found between the isotopic
608 composition of condensation water in the inner cave sectors and dripwater. This
609 suggests that the water condensation process in areas more distant from the cave
610 entrance is sourced by autochthonous water vapor. Given that the isotopic
611 composition of condensation water though the seasonal cycle is indistinguishable from
612 that of seepage water in the cave, we conclude that oxygen and hydrogen isotopes
613 are not useful in identifying the origin (condensation vs. seepage) of the droplets with
614 no apparent dripping that cover the ceiling of the *Polychrome Hall.* Also, we found that
615 the analytical precision of the current CRDS isotope analyzers to measure triple
616 oxygen isotope anomalies in waters is not enough to resolve the small seasonal
617 variations expected for cave waters (tens per meg).

618 The varying contributions of the allochthonous and autochthonous water vapor
619 sources for condensation in the cave can be attributed the natural cave ventilation, as
620 well as to the distance of the different chambers to the cave entrance and probably to
621 the role in the cave microclimate of the artificial metal door that separates the *Entrance*
622 *Hall* and the rest of the cave, as observed in previous studies (Gázquez et al., 2016;
623 Sainz et al., 2017). It is possible that a decrease in the airflow speed during the
624 ventilation period in this cave sector favors that water vapor from outside condenses

mostly in surfaces near the artificial door. Thus, this artificial element seems to be critical to prevent the *Polychrome Hall* and the rest of the cave from receiving additional water vapor from outside during the ventilation period. Our results are important for the management of the *Polychrome Hall*, since condensation water can contribute to the deterioration of the its exceptional rock art by washing out the ochre pigments. Additional efforts should be made to quantify and monitor condensation processes in Altamira Cave in forthcoming years.

Acknowledgments

The authors are grateful to the Altamira Cave Research Centre and Museum staff for their help and support during the sampling surveys in the cave. This work was supported by the Ministry of Education, Culture and Sport of Spain (MECD) [grant number J180052] under the Project “Servicio de control y seguimiento de las condiciones ambientales y del biodeterioro de la Cueva de Altamira”, and also with the support of the Cantabrian International Institute for Prehistoric Research (IIIPC) under the project entitled “Control y seguimiento de las condiciones ambientales, del agua de infiltración y de las emisiones de gas radon, de la cueva de Altamira”. The authors thanks Professor David A. Hodell for the isotopic analysis of 15 water samples. Dr. Fernando Gázquez was financially supported by the HIPATIA research program of the University of Almería and by a Ramón y Cajal Fellowship (RYC2020-029811-I) of the Spanish Government (Ministerio de Economía y Competividad). The authors are grateful to four anonymous reviews, who contributed to improve the original manuscript.

7. References

Aravena, R., Suzuki, O., Polastri, A., 1989. Coastal fogs and their relation to groundwater. Chem. Geol. 79, 83–91.

Aron, P. G., Levin, N.E., Beverly, E.J., Huth, T.E., Passey, B.H., Pelletier, E, M., Poulsen, C, J., Winkelstern, I., Yarian, D. 2021. Triple oxygen isotopes in the water cycle. Chem. Geol. 565(1):120026.

Auler, A.S., Smart, P.L., 2004. Rates of condensation corrosion in speleothems of semi-arid northeastern Brazil. Speleogenesis Evol. Karst Aquifers 2 (2) (2 pp.).

Barkan, E., Luz, B., 2005. High precision measurements of $^{17}O/^{16}O$ and $^{18}O/^{16}O$ ratios in H_2O. Rapid Commun. Mass Spectrom. 19, 3737–3742.

Barkan, E., Luz, B., 2007. Diffusivity fractionations of $H_2{}^{16}O/H_2{}^{17}O$ and $H_2{}^{16}O/H_2{}^{18}O$ in air and their implications for isotope hydrology. Rapid Commun. Mass Spectrom. 21, 2999–3005.

Bowen, G.J., Cai, Z., Fiorella, R.P., Putman, A.L., 2019. Isotopes in the Water Cycle: Regional- to Global-Scale Patterns and Applications. Ann. Rev. Earth Plant. Sci. 47, 453-479.

Calaforra, J.M., 1996. Contribución al conocimiento de la karstología de yesos (PhD Thesis). University of Granada, Spain (350 pp.).

Calaforra, J.M., Dell'Aglio, A., Forti, P., 1993. Preliminary data on the chemical erosion in gypsum karst. The Sorbas region (Spain). Proceedings of the 11th International Congress of Speleology (Beijing), pp. 97–99.

Cappa, C.D., Hendricks, M.B., DePaolo D.J., Cohen, R.C. 2003. Isotopic fractionation of water during evaporation. J. Geophys. Res., 108(D16), 4525.

672 Clark, I.D., Fritz, P., 1997. Environmental Isotopes in Hydrogeology. Lewis
673 Publishers, USA.

674 Craig, H., Gordon, L., Horibe Y., 1963. Isotopic exchange effects in the evaporation
675 of water: 1. Low-temperature experimental results. J. Geophys. Res. 68, 5079–
676 5087.

677 Cuezva, S., Sánchez-Moral, S., Saiz-Jiménez, C., Cañaveras, J.C., 2009. Microbial
678 communities and associated mineral fabrics in Altamira Cave. Spain. Int. J.
679 Speleol. 38 (1), 83-92.

680 Cuezva, S., Fernández-Cortés, A., Benavente, D., Serrano-Ortíz, P., Kowalski, A.S.,
681 Sánchez-Moral, S., 2011. Short-term CO_2(g) exchange between a shallow
682 karstic cavity and the external atmosphere during summer: Role of the surface
683 soil layer. Atmos. Environ. 45, 1418-1427.

684 De Freitas, C.R., Schmekal, A.A., 2003. Condensation as a microclimate process:
685 measurement, numerical simulation and prediction in the Glowworm tourist cave,
686 New Zealand. Int. J. Climatol. 23, 557–575.

687 De Freitas, C.R., Schmekal, A., 2006. Studies of corrosion/condensation process in
688 the Glowworm Cave, New Zealand. Int. J. Speleol. 35, 75–81.

689 Dreybrodt, W., Gabrovšek, F., Perne, M., 2005. Condensation corrosion: a
690 theoretical approach. Acta Carsol. 34, 317–348.

691 Dublyansky, V.N., Dublyansky, Y.V., 1998. The problem of condensation in karst
692 studies. J. Caves Karst Stud. 60 (1), 3–17.

693 Dublyansky, V.N., Dublyansky, Y.V., 2000. The role of condensation in karst
694 hydrogeology and speleogenesis. In: Klimchouk, A.B., Ford, D.C., Palmer, A.N.,

695 Dreybrodt, W. (Eds.), Speleogenesis, Evolution of Karst Aquifers. National
696 Speleological Society, Huntsville, pp. 100–111.

697 Elez, J., Cuezva, S., Fernández-Cortés, A., García-Antón, E., Benavente, D.,
698 Cañaveras, J.C., Sánchez-Moral, S., 2013. A GIS-based methodology to
699 quantitatively define an Adjacent Protected Area in a shallow karst cavity: case
700 of Altamira cave. J. Environ. Manage. 118, 122-124.

701 Fernández-Cortés, A., Calaforra, J.M., García-Guinea, J., 2006. The Pulpí gigantic
702 geode (Almería, Spain): geology, metal pollution, microclimatology and
703 conservation. Environ. Geol. 50, 707–716.

704 Gabrovšek, F., Dreybrodt, W., Perne, M., 2010. Physics of condensation corrosion
705 in caves. In: Andreo, B., Carrasco, F., Durán, J.J., LaMoreaux, J.W. (Eds.),
706 Advances in Research in Karst Media, Environmental Earth Sciences, pp. 491–
707 496.

708 Gázquez, F., Calaforra, J.M., Forti, P., DeWaele, J., Sanna, L., 2015a. The role of
709 condensation in the evolution of dissolutional forms in gypsum caves: study case
710 in the karst of Sorbas (SE Spain). Geomorphology, 229, 100–111.

711 Gázquez, F., I. Mather, J. Rolfe, N. P. Evans, D. Herwartz, M. Staubwasser, D. A.
712 Hodell., 2015b. Simultaneous analysis of $^{17}O/^{16}O$, $^{18}O/^{16}O$ and $^{2}H/^{1}H$ of gypsum
713 hydration water by cavity ringdown laser spectroscopy. Rapid Commun. Mass
714 Spectrom. 21, 1997–2006.

715 Gázquez, F. Quindós-Poncela, L., Sainz, C., Fernández, A., Fuentes, I., Celaya, S.,
716 2016. Spatiotemporal distribution of $\delta^{13}C$-CO_2 in a shallow cave and its potential
717 use as indicator of anthropic pressure. J. Environ. Manage. 180, 421 - 432.

718 Gázquez, F., Rull, F., Sanz-Arraz, A., Medina, J., Calaforra, J.M., de las Heras, C.,
719 Lasheras, J.A., 2017a. In situ Raman characterization of minerals and
720 degradation processes in a variety of cultural and geological heritage sites.
721 Spetrochim. Acta Part B. 172, 48-57.

722 Gázquez, F., Calaforra, J.M., Evans, N.P., Hodell, D.A., 2017b. Using stable isotopes
723 (δ ^{17}O, δ ^{18}O and δD) of gypsum hydration water to ascertain the role of water
724 condensation in the formation of subaerial gypsum speleothems. Chem. Geol.
725 452, 34–46.

726 Gázquez, F., Morellón, M., Bauska, T., Herwartz, D., Surma, J., Moreno, A.,
727 Staubwasser, M., Valero-Garcés, B., Delgado-Huertas, A., Hodell, D.A., 2018.
728 Triple oxygen and hydrogen isotopes of gypsum hydration water for quantitative
729 paleo-humidity reconstruction. Earth Planet. Sci. Lett. 481, 177–188.

730 García-Antón, E., Cuezva, S., Jurado, V., Porca, E., Miller, A.Z., Fernández-Cortés,
731 A., Saiz-Jiménez, C., Sánchez-Moral, S., 2013. Combining stable isotope (δ^{13}C)
732 of trace gases and aerobiological data to monitor the entry and dispersion of
733 microorganisms in caves. Environ. Sci. Poll. Res. 21, 473-484.

734 García-Antón, E., Cuezva, S., Fernández-Cortés, A., Benavente, D., Sánchez-Moral,
735 S., 2014. Main drivers of diffusive and advective processes of CO_2-gas exchange
736 between a shallow vadose zone and the atmosphere. Int. J. Greenh. Gas. Con.
737 21, 113-129.

738 Giménez, R. Bartolomé, M., Gázquez, F., Iglesias, M., Moreno, A. 2021. Underlying
739 climate controls in triple oxygen (^{16}O, ^{17}O, ^{18}O) and hydrogen (^{1}H, ^{2}H) isotopes
740 composition of rainfall (Central Pyrenees). Front. Earth Sci. 9, 633698.

741 Horita, J., Wesolowski, D.J., 1994. Liquid–vapor fractionation of oxygen and
742 hydrogen isotopes of water from the freezing to the critical temperature.
743 Geochim. Cosmochim. Acta 58, 3425–3437.

744 Hoyos, M., Bustillo, A., Garcia, A., Martin, C., Ortiz, R., Suazo, C., 1981.
745 Características geológico-kársticas de la cueva de Altamira (Santillana del Mar,
746 Santander). Informe Ministerio de Cultura, Madrid, 81 pp.

747 IAEA/WMO (2021). Global Network of Isotopes in Precipitation. The GNIP Database.
748 Accessible at: http://www.iaea.org/water.

749 Ingraham, N.L., Matthews, R.A., 1988. Fog drip as a source of groundwater recharge
750 in northern Kenya. Water Resour. Res. 24, 1406–1410.

751 Ingraham, N.L., Matthews, R.A., 1990. A stable isotopic study of fog: the Point Reyes
752 Peninsula, California, U.S.A. Chem. Geol. 80, 281–290.

753 Kaseke, K.F., Wang, L., Seely M.K. 2017. Nonrainfall water origins and formation
754 mechanisms. Sci. Adv. 3, e1603131.

755 Klimchouk, A.B., 1996. Speleogenesis in gypsum. Int. J. Speleol. 25 (3–4), 61–82.

756 Klimchouk, A.B., Aksem, S.D., 2002. Gypsum karst in the western Ukraine:
757 Hydrochemtry and solution rates. Carbonate Evaporite 17, 142–153.

758 Landais, A., Barkan, E., Yarik, D., Luz, B., 2006. The triple isotopic composition of
759 oxygen in leaf water. Geochim. Cosmochim. Acta. 70, 4105-4115.

760 Liñan, C., Benavente, J., del Rosal, Y., Vadillo, I., Ojeda, L., Carrasco, F., 2021.
761 Condensation water in heritage touristic caves: isotopic and hydrochemical data
762 and a new approach for its quantification through image analysis. Hydrolocial
763 Processes. doi: 10.1002/hyp.14083. in press.

764 Luz, B., Barkan, E., 2005. The isotopic ratios $^{17}O/^{16}O$ and $^{18}O/^{16}O$ in molecular
765 oxygen and their significance in biogeochemistry. Geochim. Cosmochim. Acta
766 69, 1099–1110.

767 Luz, B., Barkan, E., 2010. Variations of $^{17}O/^{16}O$ and $^{18}O/^{16}O$ in meteoric waters.
768 Geochim. Cosmochim. Acta 74, 6276–6286.

769 Luz, B., Barkan, E., Yam, R., Shemesh, A., 2009. Fractionation of oxygen and
770 hydrogen isotopes in evaporating water. Geochim. Cosmochim. Acta 73, 6697–
771 6703.

772 Pike, A.W.G., Hoffmann, D.L., García-Idez, M., Pettitt, P. B., Alcolea, J., Balbín, R.D.,
773 Gónzalez-Saiz, C., De las Heras, C., Lasheras, J.A., Montes, R., Zilhao, J., 2012.
774 U-Series Dating of Paleolithic Art in 11 Caves in Spain. Science 336 (6087),
775 1409-1413.

776 Uechi, Y., and Uemura, R., 2019. Dominant influence of the humidity in the moisture
777 source region on the 17O-excess in precipitation on a subtropical island. Earth
778 Planet. Sci. Lett. 513, 20–28.

779 Quindós, L.S., Bonet, A., Daz-Caneja, N., Fernandez, P.L., Gutierrez, I., Solana, J.R.
780 Soto, J., Villar, E., 1987. Study of the environmental variables affecting the
781 natural preservation of the Altamira Cave paintings located at Santillana del Mar,
782 Spain. Atmos. Environ. 21(3), 551-560.

783 Sainz, C., Rábago, D., Celaya, S., Fernandez, E., Quindós, J., Quindós, L,
784 Fernández, A., Fuente, I., Arteche, J.L., Quindós, L.S., 2017. Continuous
785 monitoring of radon gas as a tool to understand air dynamics in the cave of
786 Altamira (Cantabria, Spain). Sci. Total Environ. 624, 416-423.

Sarbu, S.M., Lascu, C., 1997. Condensation Corrosion in Movile Cave, Romania. J. Caves Karst Stud. 59, 99–102.

Schoenemann, S. W., Schauer, A. J., Steig, E. J., 2013. Measurement of SLAP2 and GISP $\delta^{17}O$ and proposed VSMOW-SLAP normalization for $\delta^{17}O$ and $^{17}O_{excess}$. Rapid Commun. Mass Spectrom. 27, 582–590.

Steig, E. J., Gkinis, V., Schauer, A. J., Schoenemann, S. W., Samek, K., Hoffnagle, J., Dennis K.J., Tan, S.M., 2014. Calibrated high-precision ^{17}O-excess measurements using cavity ring-down spectroscopy with laser-current-tuned cavity resonance. Atmos. Meas. Tech. 7, 2421–2435.

Surma, J., Assonov, S., Staubwasser, M., 2021. Triple Oxygen Isotope Systematics in the Hydrologic Cycle. Rev. Mineral. Geochem. 86(1):401-428.

Tarhule-Lips, R.F.A., Ford, D.C., 1998. Condensation corrosion in caves on Cayman Brac and Isla de Mona. J. Caves Karst Stud. 60, 84–95.

Tian, C., Wang, L., Kaseke, K.F., Bird, B.W., 2018. Stable isotope compositions (d2H, d18O and d17O) of rainfall and snowfall in the central United States. Sci. Rep. 8, 6712.

Voigt, C., Herwartz, D., Dorador, C., Staubwasser, M. 2021. Triple oxygen isotope systematics of evaporation and mixing processes in a dynamic desert lake system. Hydrol. Earth Syst. Sci., 25, 1211–1228.

Wassenaar, L., Terzer-Wassmuth, S., Douence, C. Progress and challenges in dual- and triple-isotope (δ18O, δ2H, Δ17O) analyses of environmental waters: An international assessment of laboratory performance. Rapid Commun Mass Spectrom. 35(24):e9193.

White, J.H., Dominguez-Villar, D., Hartland, A., 2021. Condensation corrosion alters the oxygen and carbon isotope ratios of speleothem and limestone surfaces. Res. Geochem., e100008.

The role of cave ventilation in the triple oxygen and hydrogen isotope composition of condensation waters in Altamira Cave, northern Spain

Fernando Gázquez[1,2*], Luis Quindós[3,4], Daniel Rábago[3], Ismael Fuente[3], Santiago Celaya[3], Carlos Sainz[3,4]

(1) Department of Biology and Geology, Universidad de Almería, Carretera de Sacramento s.n, La Cañada de San Urbano, Almería, 04120, Spain.

(2) Andalusian Centre for the Monitoring and Assessment of Global Change (CAESCG), University of Almería, Spain

(3) Radon Research Group. Faculty of Medicine. University of Cantabria, Avda. Cardenal Herrera Oria s/n E-39011 Santander, Spain.

(4) The Cantabrian International Institute for Prehistoric Research (IIIPC)

*Corresponding author (f.gazquez@ual.es)

Abstract

In cave environments, water vapor condensation occurs naturally when warmer/wet air masses flow close to colder cave surfaces. Artificial microclimate perturbations in show caves can enhance this process, leading to potential deterioration of rock art and degradation of speleothems. Here we investigate the triple oxygen and hydrogen isotopic compositions of condensation water in Altamira Cave (Cantabria, northern Spain) to evaluate the potential of stable isotopes in the study of condensation mechanisms in caves. We assess the role of cave ventilation in the spatiotemporal isotopic variability of condensation water in Altamira Cave. To this end, water drops that condense naturally on artificial supports in different parts of the cave were

collected for 7 years and their isotopic compositions ($\delta^{17}O$, $\delta^{18}O$, δD and derived parameters ^{17}O-excess and d-excess) were compared to those of droplets with no apparent dripping taken from the cave ceiling (i.e. presumably condensation water) and fast dripping points (i.e. infiltration water) during the same period. Condensation waters in the outmost cave sectors, closer to the entrance, show higher $\delta^{17}O$, $\delta^{18}O$ and δD values during the cave ventilation period (June to October) compared to the rest of the year. This seasonal pattern can be explained by changes in the contributions of two moisture sources for condensation: advection of allochthonous water vapor from outside during the cave ventilation period and recycling of autochthonous vapor generated from cave dripwater during the stagnation period. In contrast, the isotopic values of condensation waters in the inner cave sectors are similar to those of infiltration water, with insignificant seasonal variability. This suggests that water condensation in the inner cave sectors is sourced by autochthonous vapor, with no significant contributions of external moisture, even during the cave ventilation period. We conclude that allochthonous water vapor condenses preferentially in the *Entrance Hall* and does not affect significantly the rest of the cave. These results are relevant for the management of Altamira Cave and for future investigations on condensation mechanisms in cavities elsewhere.

Keywords: cave management, cave monitoring, condensation water, stable isotopes, oxygen-17, triple oxygen isotopes.

1. Introduction

The prehistoric paintings of the *Polychrome Hall* of Altamira Cave are the maximum expression of the Paleolithic rock art in the Iberian Peninsula. This cave hosts

49 priceless rock art paintings, some 36,160 – 15,329 cal. BP that have earned it the
50 name “Sistine Chapel” of the Paleolithic, due to the reddish and ochre-colored bison
51 and deer paintings that cover the ceiling of the renowned *Polychrome Hall* (Pike et al.,
52 2012; Gázquez et al., 2017a) (Fig. 1). The cave was declared World Heritage Site by
53 the UNESCO in 1985 (http://whc.unesco.org/en/list/310) and was recently reopened
54 to the public under an extremely restrictive visitor regime (Gázquez et al., 2016, 2017a;
55 Sainz et al., 2017). Preserving the integrity of these and others rock art features from
56 natural and anthropic perturbations is a priority in the management of show caves.

57 Among the several threats to the rock art heritage, resuspension and mobilization of
58 pigments (mostly ochres and charcoal) by cave water, including seepage and
59 condensation waters, are major hazards. Water films and drops can accumulate in
60 some parts of the cave walls and ceilings. Identifying the source of water
61 (condensation vs. infiltration) is crucial to develop protocols devoted to minimize the
62 impact on the cave features, including rock art and speleothems (Dublyansky and
63 Dublyansky, 2000; Fernández-Cortés et al., 2006).

64 The largest intakes of external water vapor in Altamira Cave may occur during the
65 cave ventilation period (June to October) (Quindós et al., 1987; Cuezva et al., 2009;
66 García-Antón et al., 2013; Gázquez et al., 2016b; Sainz et al., 2017), when relatively
67 warm and moist air masses enter the cave and cool, forcing condensation. In order to
68 reduce the inputs of airborne particles (i.e. organic matter, fungi and bacteria) that
69 could deteriorate the Paleolithic rock art of Altamira Cave, an artificial metal door was
70 installed in 2008 between the *Entrance Hall* (~20 m apart from the entrance) and the
71 rest of the cave. This intervention has had a positive impact on the microclimate
72 stability of the inner cave sectors in terms of temperature stability and decrease in
73 airborne particles (Sainz et al., 2018); however, the role of this artificial barrier in the

condensation processes in the cave has not been investigated to date. Indeed, specific studies on water condensation in Altamira Cave have not been performed yet.

Direct measurements of the condensation/evaporation processes have been conducted previously in caves worldwide by using suspended glass plates (Sarbu and Lascu, 1997), lysimeters and metallic devices (Dublyansky and Dublyansky, 1998; Gázquez et al., 2015a; 2017b) and refrigerated containers (Tarhule-Lips and Ford, 1998; Liñán et al., 2021), in order to quantify the magnitude of these mechanisms. Electrical devices coupled to data loggers have been utilized also to quantify condensation in caves (De Freitas and Schmekal, 2006). In addition, indirect measurements of the effects of condensation have been conducted by monitoring weight loss of rock tablets (Calaforra, 1996; Klimchouk et al., 1996; Tarhule-Lips and Ford, 1998; Klimchouk and Aksem, 2002; White et al., 2021), using micro-erosion meter measurements of cave surface retreatment (Calaforra and Forti, 1993; Klimchouk et al., 1996; Gázquez et al., 2015a) and determining thickness and age of weathering rinds (Auler and Smart, 2004). Indirect estimates of condensation/evaporation can be also obtained from microclimate monitoring of cave atmosphere and rock temperatures (De Freitas et al., 2003; Fernández-Cortés et al., 2006). Furthermore, theoretical approaches to the condensation mechanisms in caves have been developed in the last decades (Dreybrodt et al., 2005; Gabrovšek et al., 2010). More recently, thermal image analyses have been used to quantify condensation-evaporation processes in caves (Liñán et al., 2021).

The oxygen and hydrogen isotopes composition of water [$^{18}O/^{16}O$ and $^{2}H/^{1}H$ or $\delta^{18}O$ and δD, respectively, when standardized to the international water standard Vienna-Standard Mean Ocean Water (V-SMOW)] has been widely used to track a variety of processes in the hydrosphere (Bowen et al., 2019 and references therein), including

recent preliminary studies of condensation water in caves by Liñán et al. (2021). These authors found that condensation waters in Nerja Cave, southern Spain, display higher $\delta^{18}O$ and δD values and lower d-excess values during the cave ventilation periods than during the rest of the year. This seasonal pattern was attributed to the impact of evaporation on condensation water, which takes place during the cave ventilation period because of low relative humidity in the cave atmosphere (60-80%).

In addition to the traditional measurements of $\delta^{18}O$ and δD in waters, recent analytical advances have permitted obtaining precise measurements of the triple oxygen isotope composition ($\delta^{17}O$ and $\delta^{18}O$) (Barkan and Luz, 2005; Steig et al., 2014). The $\delta^{17}O$ deviations with respect to the $\delta^{17}O$–$\delta^{18}O$ Global Meteoric Water Line (GMWL), which has a proposed slope of 0.528, are expressed as ^{17}O-excess [$^{17}O\text{-excess} = \ln(\delta^{17}O/1000 + 1) - 0.528 \ln(\delta^{18}O/1000 + 1)$] (Barkan and Luz, 2005; Luz and Barkan, 2010). This reference slope is commonly used to express triple oxygen deviation in the hydrological cycle (Aron et al., 2021; Surma et al., 2021).

The ^{17}O-excess parameter in rainfall has been found to be sensitive to variations in relative humidity at the moisture source, with smaller temperature dependence than d-excess (d-excess=$\delta D - 8 * \delta^{18}O$) (Barkan and Luz, 2005, 2007; Luz and Barkan, 2010; Uechi and Uemura, 2019). Likewise, other parameters, including raindrop re-evaporation and moisture recycling during water vapor transport can modulates the final ^{17}O-excess signal of rainwater (Tian et al., 2018; Giménez et al., 2021). Thus, measuring the triple oxygen and hydrogen isotope composition of water can help to track environmental conditions (e.g. temperature vs. relative humidity) during water phase changes and during transport of water vapor masses (Aron et al., 2021; Surma et al., 2021).

Here, we conducted a 7-years monitoring study of stable isotopes ($\delta^{17}O$, $\delta^{18}O$, $\delta^{2}H$ and derived parameters d-excess and ^{17}O-excess) in condensation water and dripwater in Altamira Cave. We aim to identify isotopic differences between seepage and condensation water, in order to assess whether the numerous droplets observed in the ceiling of the *Polychrome Hall* of Altamira Cave are associated with either condensation or infiltration water. In addition, we investigate the origin of vapor for water condensation and the spatiotemporal pattern of the condensation mechanisms in this cave. To this end, we analyzed waters deposited on artificial supports in several locations of the cavity, as well as dripwater from fast drips (i.e. discharge point related to seepage of meteoric water) and ceiling droplets with no apparent dripping (presumably associated with water condensation) in the *Polychrome Hall*. The microclimate characteristics related to cave atmosphere ventilation (air temperature, relative humidity and CO_2 content) were monitored during the length of the study, in order to characterize the parameters that control the cave ventilation pattern and to identify connections with the condensation processes. We use an isotopic mixing model to demonstrate that different sources of water vapor contribute to condensation water in Altamira Cave and that the relevance of these sources change temporally and spatially.

2. Setting and cave description

Altamira Cave (43º22'37''N; 4º07'11''W) is located near the village of Santillana del Mar (Cantabria, northern Spain), at an elevation of 152 m a.s.l and 4.5 km from the Cantabrian Sea. The cavern runs NW-SE and has developed along a subhorizontal sequence of Cenomanian-Turonian marine carbonates (Hoyos *et al.*, 1981) where the

difference in level between the entrance and its deepest part (*Grave Hall*) is barely 26 m. Several cave sections can be distinguished according to their morphology and distance/depth from the entrance: the *Entrance Hall* is a ~20 m-long horizontal hall; from there, access to the rest of the cave is via an artificial door located in a narrow passage, ~2 m wide. Beyond, the cave divides along two branches. To the east is the *Polychrome Hall*, ~15 m long, ~7 m wide and up to 3 m high and lying about 2 m lower than the cave entrance. The other branch gives access to *Walls Hall*, roughly 50 m in length, 20 m wide and up to 7 m high; located ~6 m below the entrance.

A passage, roughly 60 m long runs SE-NE into the *Great Hall*. From here, artificial stairs carved in the rock lead to *Grave Hall*, lying ~15 m below the cave entrance and containing an ephemeral water pool that only appears during periods of high dripwater discharge. To the South, along a 10 m-long passage, lies the *Shower Hall*. This in turn leads into the *Well Hall*, at the depth of 12 m beneath the cave entrance. Finally, there is a meandriform sub-horizontal passage (called the *Horsetail*) approximately 40 m long that represents the innermost cave area. The thickness of the cap rock overlaying the cave varies from 2 to 18 m (Elez *et al.*, 2013) (Fig. 1). There is no permanent running watercourse inside the cave.

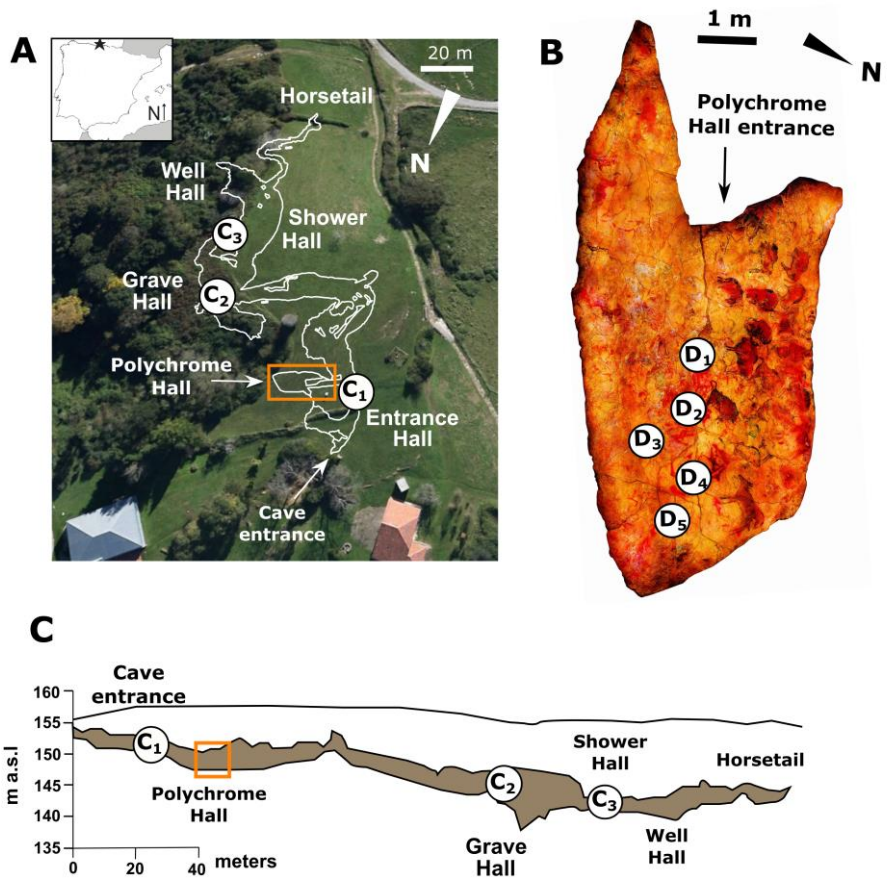

164

165 **Figure 1. A.** Location of Altamira Cave and distribution of the sampling sites in the
166 cavity, including artificial supports to collect condensation water (C1, C2 and C3); B.
167 View of the ceiling of Polychrome Hall (location is marked in orange rectangles in
168 panels 1A and 1C) with collection locations for the natural dripwater (D1) and droplets
169 (D2-D5) labelled; C. Vertical profile of Altamira Cave and location of the sampling sites
170 (modified from García-Antón et al., 2014).

171

172 The climate in this region is Oceanic (Cfb climate type, according to the Köppen
173 climate classification). The rainfall is generally abundant, exceeding 1,000 mm/year.
174 July is the driest month (30 mm on average) and the rainiest period occurs from
175 October to December (Fig. 2). The mean external air temperatures are minimum in

January (9 °C) and maximum in July (21 °C). The vegetation coverage over the cave is dominated by grasses with minor presence of scrubs and trees (Fig. 1A).

Altamira Cave has a relatively stable microclimate, with air temperatures that vary less than 2 ^{o}C throughout the year in the innermost areas (*Well Hall* and *Horsetail*) and up to 5 ^{o}C in the outermost part of the cave (*Entrance Hall*) (Gázquez et al., 2016). The mean temperature in the *Polychrome Hall* during the period of study was 14.2±0.5 ^{o}C (maximum value of 15 ^{o}C and minimum value of 13.2 ^{o}C).

The air temperature and ventilation regime of Altamira Cave are fundamentally controlled by the annual thermal oscillations of the outside air temperature and the water saturation of the epikarst and the soil over the cave (Cuezva et al., 2011). The outside temperature oscillations are transmitted into the cave through the rock, which attenuates its amplitude and causes a lag between the outer thermal wave and the temperature of the subterranean atmosphere (Elez et al., 2013). Consequently, the cave ventilation period occurs in summer (June to October), while the cave stagnation period takes place in winter (November to May). The annual variation of in-cave air temperature exhibits a sinusoidal pattern with a thermal lag time (~2 months on average) between the innermost and outermost cave areas that depends on the outside temperature and the thickness of the rock over the different cave sectors (Quindós et al., 1987; Cuezva et al., 2011; Sainz et al 2017).

3. Methods

We assess the spatial gradient and temporal variability of the isotopic composition of condensation water and dripwater, as well as cave environmental parameters (air temperature, relative humidity and CO_2 content) in Altamira Cave, by monitoring and

repeatedly sampling from the cave entrance to more stable locations deeper within the cave.

3.1. Water sampling

From November 2014 to March 2017, condensation water that accumulates on a metallic door that separates the Entrance Hall and the rest of the cave (site C1 in Fig. 1) was collected using disposable pipets (~200 μl) (n=11). From March 2017 to October 2020, sampling was conducted approximately every two weeks in the same location, but condensation was collected from the metal support of a thermometer that is 1 m apart from the door. In addition, condensation water from two inner cave locations (sites C2 and C3 in Fig. 1) was collected from metal supports of thermometers using the same method from March 2017 to August 2020. Water samples were stored at 4 ^{o}C in 2 ml glass tubes provided with a micro-insert (~300 μl; Thermo Fisher, n. 10376102) and capped with silicone septum caps. A total of 76 surveys were conducted and a total of 192 condensation water samples from artificial supports were collected.

Dripwater samples from a relatively fast discharge point (maximum of 143 ml/day; mean of 61±21 ml/day) in the *Polychrome Hall* (site D1 in Fig. 1) were collected approximately every two weeks between March 2017 and August 2020. A graduated container was placed under the drip point and volumes were recorded between surveys in order to calculate drip rates. Water samples were collected from this container and stored in 14 ml glass tubes at 4 ^{o}C. A total of 76 dripwater samples were collected from site D1. In addition, water droplets from four selected locations of the ceiling of the *Polychrome Hall* (i.e., sites with no visibly dripping; D2-D5 in Fig. 1) were collected and stored using the same protocol as for condensation water. A total of 254

samples from these four locations were taken every two weeks between March 2017 and October 2020.

3.2. Stable isotopes analysis

Samples collected between July 2013 and July 2014 were analyzed for $\delta^{18}O$ and δD using a L1102-i Picarro water isotope analyzer at the Godwin Laboratory for Paleoclimate Research, University of Cambridge, UK. Samples collected between August 2014 and October 2020 were analyzed for $\delta^{17}O$, $\delta^{18}O$ and δD at the Laboratory of Stable Isotopes of the University of Almeria, Spain using a L2140-i Picarro water isotope analyzer (Picarro, Inc., Santa Clara, California, USA).

Each sample was injected ten times into the vaporizer (A0211 manufactured by Picarro, Inc.), which was heated to 110°C. Potential contamination produced by organic compounds in water, which may affect specially the measurements of ^{17}O-excess values, was removed by using a Picarro micro-combustion module (MCM) coupled to the L2140-i Picarro analyzer (Gázquez et al., 2015b). Memory effects from previous samples were avoided by rejecting the first three analyses. Values for the final 7 injections were averaged with a typical mean instrumental precision (±1SD) of ±0.02‰ for $\delta^{17}O$, ±0.03‰ for $\delta^{18}O$ and ±0.19‰ for δD when using the L2140-i Picarro analyzer, as observed from repeated analysis of an in-house water standard (n=54) together with the water samples. The instrumental precision of the L1102-i Picarro analyzer was ±0.05‰ for $\delta^{18}O$ and ±0.6‰ for δD. The in-run drift of the instruments was monitored by analyzing a water standard (BOTTY) every 6 samples. The results were normalized against V-SMOW-SLAP in the case of triple oxygen isotopes, and against V-SMOW-SLAP-GISP in the case of hydrogen isotopes, by analyzing internal

standards before and after each set of fifteen to twenty samples (see Supplementary Table 1 for examples of our calibration). To this end, three internal water standards (JRW, $\delta^{17}O$=-9.99‰, $\delta^{18}O$=-18.90‰ and δD=-146.5‰; BOTTY, $\delta^{17}O$=-3.88‰, $\delta^{18}O$=-7.40‰ and δD=-50.38‰; SPIT, $\delta^{17}O$=-0.09‰, $\delta^{18}O$=-0.15‰ and δD=-0.44‰) were calibrated previously for triple oxygen isotopes against V-SMOW and SLAP by a two-points calibration, using $\delta^{17}O$ of 0.0‰ and -29.69865‰, respectively, and $\delta^{18}O$ of 0.0‰ and -55.5‰, respectively (Schoenemann et al., 2013). This approach assumes V-SMOW and SLAP have ^{17}O-excess= 0. The δD of the internal standards was calibrated against V-SMOW, GISP and SLAP using a three-points calibration. Note that GISP does not have an accepted $\delta^{17}O$ value, so cannot be used for triple oxygen isotope calibration. Instead, the GISP water standard was analyzed as an unknown during the calibration of our internal standards, yielding an average ^{17}O-excess value of 19±18 per meg. This value is in good agreement with the results reported by previous studies (e.g. Schoenemann et al. 2013; 22±11 per meg).

The ^{17}O-excess was calculated for each injection using the normalized $\delta^{17}O$ and $\delta^{18}O$ values. The final reported value is the average of ^{17}O-excess values from all 7 suitable injections. All ^{17}O-excess values are given in per meg units (1 per meg = 0.001‰). Typical in-sample ^{17}O-excess and d-excess precisions (1SD) in water standards (BOTTY, n=54), were 13 per meg and 0.2‰, respectively, similar to the precision obtained by other CRDS instruments (Wassermann et al., 2021).

3.3. Microclimate monitoring

Measurements of air temperature and air CO_2 concentrations were conducted at sites C1, C2 and C3, in the *Polychrome Hall* (Fig. 1) and outside the cave close to the

entrance door, between January 2014 and October 2020. Rainfall amount was recorded by a meteorological station located in the terrain over the cave during the length of the study. A total of 191 monitoring campaigns were conducted during this period, typically every two weeks and between 10 a.m. and 12 p.m. The in-cave temperature measurements used mercury thermometers with a precision of ±0.05 ^{o}C that were installed in the cave at the beginning of this study. For the measurements of the external air we used a portable digital temperature probe (Vaisala HMP155) with a precision of ±0.1 ^{o}C. The concentration of CO_2 in air was analyzed in situ using a Testo 445 (mod. 0560-4450) device with a precision of 5%. Relative humidity was measured using EE21 Series instrument, with an accuracy of ±3%. Additionally, the automatic measurements performed by this device have being reproduced with grab sampling measurements carried out with an aspiration psicrometer Lambrecht kG Göttingen (model 761), with a resolution of 2%.

3.4. Stable isotope modeling

We modeled the stable isotope composition of condensation water at site C1 by using a two-endmember mixing model, in which the endmembers are the water vapor generated within the cave (autochthonous water vapor hereafter) and the water vapor that enters the cave from outside during the cave ventilation period (allochthonous water vapor hereafter) (see Supplementary Table 2 for model parametrization and calculations). The CO_2 content in air is assumed to reflect the degree of atmosphere ventilation at site C1. This means that the maximum CO_2 content recorded at site C1 during the cave stagnation period (5525 ppm) represents 0% ventilation and the outside CO_2 content during the length of this study (470 ppm) represents 100% ventilation. We assume a linear relationship between the CO_2 content and the degree

297 of cave ventilation at site C1. The isotopic composition of the two water vapor
298 reservoirs can be approximated by assuming equilibrium conditions with
299 environmental water (i.e. cave water and meteoric water). We use the mean isotopic
300 composition of dripwater at site D1 to represent the isotopic composition of cave water
301 ($\delta^{18}O$ = -5.9±0.1‰, δD= -32.8±0.4‰, d-excess= 14.4±0.6‰, ^{17}O-excess = 25±7 per
302 meg, during the length of this study). We use the long-term (i.e. 15 years mean)
303 monthly values of $\delta^{18}O$ and δD in rainfall recorded by the meteorological station of
304 Santander city, 15 km apart from Altamira Cave (data from the Global Network of
305 Isotopes in Precipitation of the International Atomic Energy Agency, period 2000-2015;
306 IAEA/WMO 2021) to calculate the isotopic composition of the external vapor. Because
307 there is no $\delta^{17}O$ data, and therefore ^{17}O-excess cannot be calculated for precipitation
308 near Altamira Cave, we assume that the ^{17}O-excess in rainfall correlates linearly with
309 $\delta^{18}O$, as reported by Giménez et al. (2021) in the Pyrenees (northern Spain), ~220 km
310 from Altamira Cave. These authors found that the $\delta^{18}O$-^{17}O-excess relationship has a
311 slope of 3.8 per meg/‰ at this site. Then, we use this relationship to calculate the ^{17}O-
312 excess of rainfall in the setting of Altamira Cave from the $\delta^{18}O$ of rainfall. Finally, the
313 $\delta^{17}O$ is calculated from $\delta^{18}O$ and ^{17}O-excess.
314 The isotopic compositions of both, the autochthonous and the allochthonous water
315 vapor are controlled by the in-cave and external temperatures, respectively.
316 Equilibrium liquid-vapor fractionation factors for $\delta^{18}O$ ($\alpha^{18}O_{eq}$) and δD (αD_{eq}) are
317 calculated here as a function of temperature using the equations of Horita and
318 Wesolowski (1994). The $\alpha^{17}O_{eq}$ is calculated as $\alpha^{17}O_{eq} = \alpha^{18}O_{eq}{}^{\theta}$, where θ is
319 0.529±0.001 (Barkan and Luz, 2005).
320

4. Results

A total of 481 water samples from Altamira Cave were analyzed for triple oxygen and hydrogen isotopes. The summary of the $\delta^{17}O$, $\delta^{18}O$, δD values and derived parameters d-excess and ^{17}O-excess are given in Table 1 and Supplementary Table 3. The results are plotted with time in Figure 2, along with the monitored climate parameters at site C1.

4.1. Condensation water from artificial supports

4.1.1. Outmost cave sector (site C1)

The $\delta^{18}O$ and δD values of condensation water from the outmost part of the cave correlate linearly (δD= 6.9(±0.2)*$\delta^{18}O$ + 9.1(±1.1); R^2=0.94, p-value<0.05). The slope of this relationship is similar to that of the Local Meteoric Water Line (δD= 7.1(±0.1)*$\delta^{18}O$ + 7.4(±0.8); R^2=0.93, p-value<0.05) in Santander city (15 km from Altamira Cave; IAEA/WMO, 2021), while the intercept is slightly higher than that of the LMWL (Fig. 3A). The d-excess and ^{17}O-excess values of condensation water at site C1 are not correlated with $\delta^{18}O$ (R^2=0.1, p-value>0.05) (Fig. 3). The $\delta^{18}O$ and δD values are higher during the cave ventilation period (-4.6±0.7‰ and -22.4±4.6‰, respectively), while during the rest of the year are lower and less variable (-5.6±0.4‰ and -30.0±3.0‰, respectively) (Fig. 2 and 4). The ^{17}O-excess values of condensation water at site C1 average 27±11 per meg and ranges from 6 to 60 per meg. No systematic differences in this parameter have been between the ventilation period (27±12 per meg) and the stagnation period (28±9 per meg), probably due to insufficient analytical precision of the measurements (±13 per meg, 1SD) (Fig. 4). The d-excess

shows more variable values during the ventilation period (14.3±2.1‰) than during the cave stagnation period (15.2±1.1‰) (Fig. 2 and 4).

4.1.2. Inner cave sectors (sites C2 and C3)

The mean $\delta^{18}O$ and δD values of condensation water from the two sites investigated in the inner part of the cave (sites C2 and C3) are indistinguishable within errors (Table 1 and Supplementary Table 3). The $\delta^{18}O$ and δD values correlate linearly ($\delta D = 4.5(\pm0.4)*\delta^{18}O - 6.0(\pm1.4)$; $R^2=0.76$, p-value<0.05) (Fig. 3). The annual variability is less than 0.3‰ (1SD) for $\delta^{18}O$ and less than 1.6‰ for δD and does not correlate with seasonal changes in the monitored air parameters (temperature and CO_2 concentration) in the cave (Fig. 2). Indeed, no significant differences in all the measured isotopic parameters can be distinguished between the cave ventilation period and the stagnation period (Table 1 and Fig. 4). The correlation between d-excess and $\delta^{18}O$ is negative and statistically significant ($R^2=0.63$, p-value<0.05) (Fig. 3). There are no significant correlations between ^{17}O-excess and $\delta^{18}O$ ($R^2=0.01$, p-value>0.05) or between ^{17}O-excess and d-excess ($R^2=0.12$, p-value>0.05) (Fig. 3).

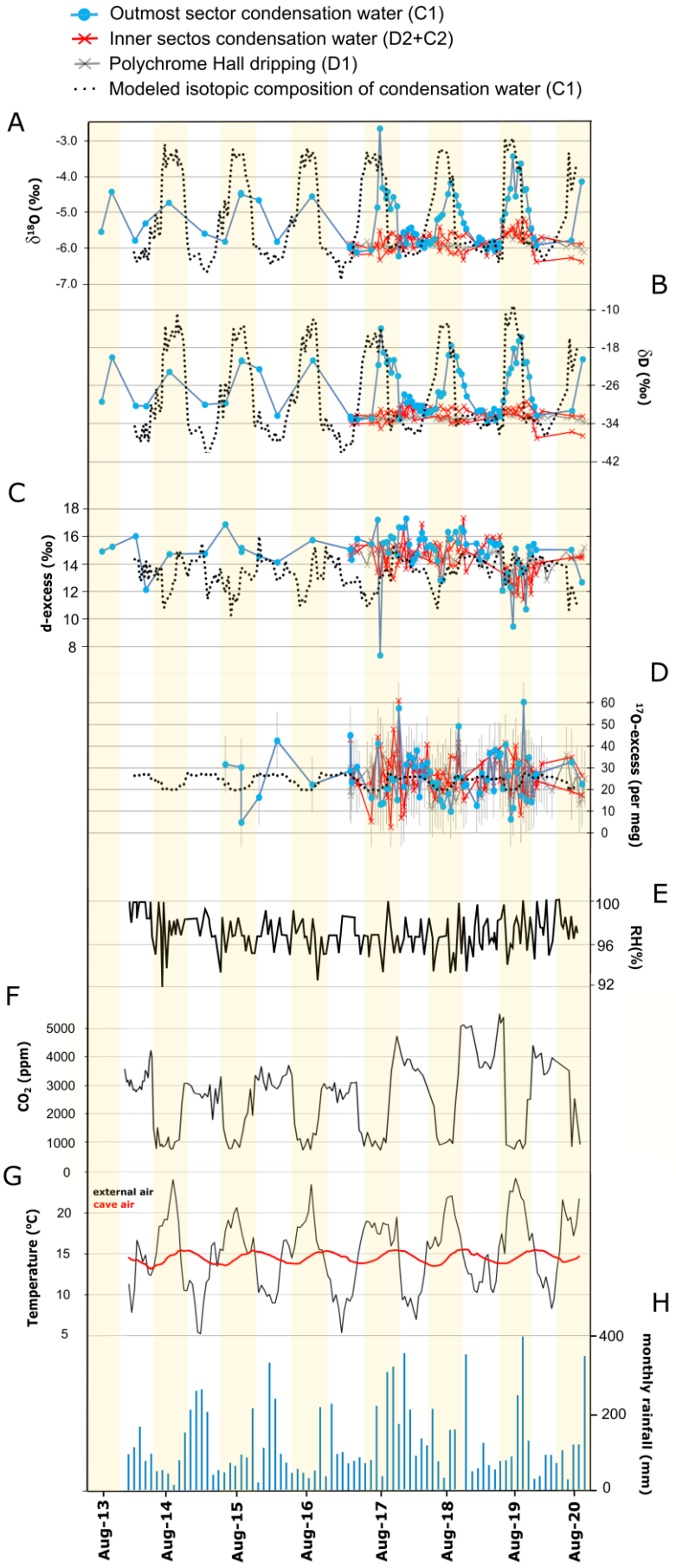
Outmost sector condensation water (C1)
Inner sectos condensation water (D2+C2)
Polychrome Hall dripping (D1)
Modeled isotopic composition of condensation water (C1)
A
δ18O (‰)
B
δD (‰)
C
d-excess (‰)
D
17O-excess (per meg)
E
RH(%)
F
CO2 (ppm)
G
Temperature (°C)
external air
cave air
H
monthly rainfall (mm)
Aug-13
Aug-14
Aug-15
Aug-16
Aug-17
Aug-18
Aug-19
Aug-20

360

Figure 2. Temporal variations of oxygen and hydrogen stable isotopes (A. $\delta^{18}O$; B. δD; C. d-excess; D. ^{17}O-excess) of condensation water and dripwater Altamira Cave (site C1 in Fig. 1). Results of modeled isotope composition of condensation water at site C1 are displayed (dashed lines). Relative humidity (E) (site C1), CO_2 concentration in the cave atmosphere (F) (site C1), air temperature in the cave (site C1) and outside (G) and monthly rainfall in Santillana del Mar (H) are presented. A 2-point moving average has been used to represent air temperature. The yellow bands represent cave ventilation periods (June to October).

4.2. Dripwater (site D1) and ceiling droplets (sites D2, D3, D4 and D5) in the *Polychrome Hall*

The $\delta^{18}O$ of the fast discharge point in the *Polychrome Hall* (site D1) ranged from -6.1 to -5.5‰, with a mean of -5.9±0.1‰. The δD ranged from -33.7 to -31.6‰, with a mean of -32.8±0.4‰. The d-excess varied between 11.9 and 15.0‰, with a mean of 14.4±0.6‰, and the ^{17}O-excess varied between 11 and 39 per meg with a mean of 25±7 per meg (Table 1). No clear systematic seasonal patterns have been observed in the isotopic parameters during the 4-years monitoring (Fig. 2 and 4).

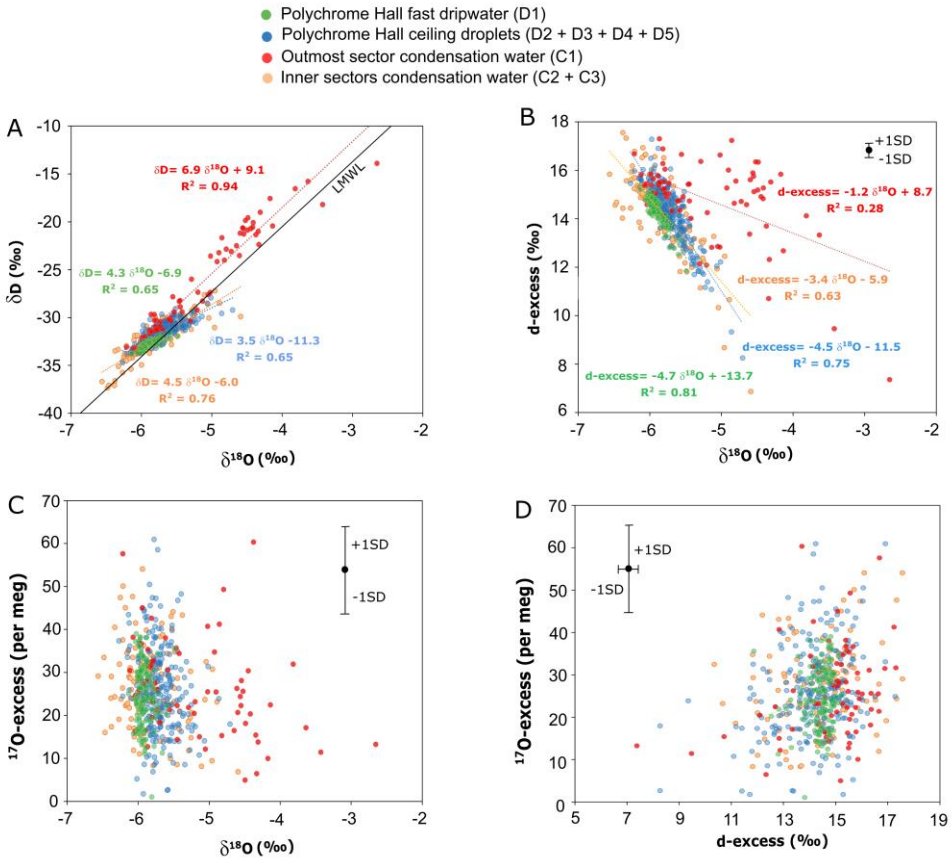

Figure 3. Cross-plot of isotopic parameters (A. δD vs. $\delta^{18}O$; B. d-excess vs. $\delta^{18}O$; C. ^{17}O-excess vs. $\delta^{18}O$; D. ^{17}O-excess vs. d-excess) in condensation waters (sites C1, C2 and C3), dripwater (D1) and ceiling droplets with no apparent dripping in the ceiling of the *Polychrome Hall* (D2, D3, D4 and D5) of Altamira Cave. The local meteoric water line (LMWL; IAEA/WMO, 2021) is given for comparison in panel A. The errors for $\delta^{18}O$ and δD are smaller than the symbols. The mean analytical errors for d-excess (0.2‰) and ^{17}O-excess (13 per meg) are represented in panels B, C and D.

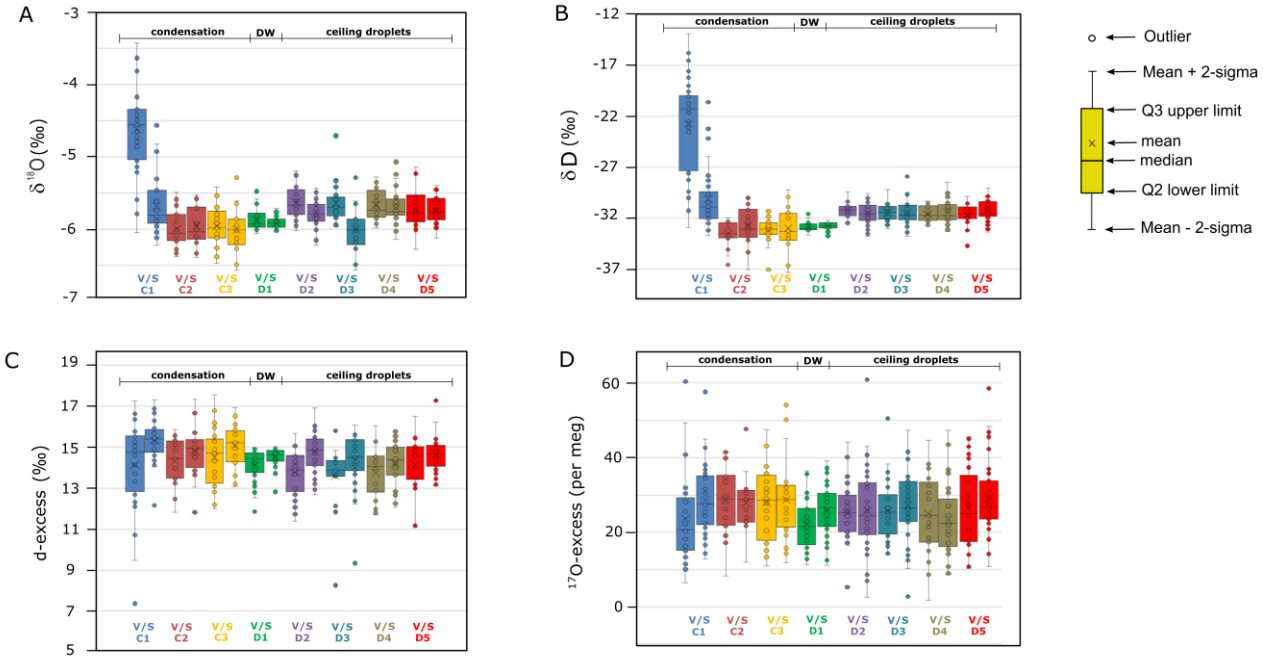

386

387 **Figure 4.** Box and whisker plots of $\delta^{18}O$ (A), δD (B), d-excess (C) and ^{17}O-excess
388 (D) of condensation water in the outmost cave sector (sites C1) and in the inner
389 sectors (sites C2 and C3), as well as dripwater (DW, site D1) and ceiling droplets
390 with no apparent dripping (sites D2, D3, D4 and D5) in the *Polychrome Hall* of
391 Altamira Cave. Results of the cave ventilation period (V; June to October) and the
392 stagnation period (S; November to May) are displayed for comparison.

393

394 The isotopic composition of the ceiling droplets with no apparent dripping in the
395 *Polychrome Hall* (D2, D3, D4, D5) are statistically indistinguishable (Table 1 and Fig.
396 4). Taking altogether, the $\delta^{18}O$ of the ceiling droplets ranged from -6.3 to -4.7‰, with
397 a mean of -5.7±0.2‰. The δD ranged from -34.7 to -27.9‰, with a mean of -31.4±1‰.
398 The d-excess varied between 8.0 and 17.3‰, with a mean of 14.2±1.3‰, and the ^{17}O-
399 excess did between 2 and 61 per meg with a mean of 26±10 per meg. No systematic
400 seasonal patterns have been observed in the isotopic parameters during the 4-years

401 monitoring (Table 1 and Fig. 4). The $\delta^{18}O$ and δD in the four points showed similar
402 patterns with time (R^2>0.4 and p-value<0.05).

403

404 **4.3. Microclimate parameters**

405 The air temperature in the *Entrance Hall* (site C1 in Fig. 1) ranged from 13.1 from 15.7
406 ºC, with a mean value of 14.5±0.6 ºC. Maximum temperatures were recorded in
407 September and minimum temperatures correspond to March. In the *Polychrome Hall*
408 (sites D1, D2, D3, D4 and D5 in Fig. 1) air temperature oscillated between 13.2 and
409 15.0 ºC and the mean value was 14.2±0.5 ºC. Maximum temperatures were recorded
410 in December, while minimum temperatures correspond to June. The temperature in
411 the innermost sector of the cave (locations C2 and C3 in Fig. 1) varied between 12.5
412 and 14.5 ºC, with a mean of 13.7±0.2 ºC. Maximum temperatures were recorded
413 between October and February and minimum temperatures corresponded to June and
414 July. The temperature outside measured during the visits to the cave (between 10 a.m.
415 and 12 p.m) ranged from 2.9 to 25.1 ºC, with a mean of 15.1±4.7 ºC. Maximum
416 temperatures outside were recorded in August, while minimum temperatures
417 correspond to January and February. August and July are the driest month of the
418 series, while the autumn and spring months concentrate most of the annual
419 precipitation (Fig. 2).

420 The mean CO_2 in the *Polychrome Hall* was 2580±1423 ppm, with lower values around
421 1000 ppm from June to October ("ventilation period") and higher values around 3000
422 ppm were recorded between November and May ("stagnation period"). At site C1, the
423 CO_2 content varied between 724 and 5525 ppm. The change from lower to higher CO_2

conditions (and vice versa) generally takes place in around 2 weeks, mainly depending on the external meteorology.

Relative humidity (RH) in the *Polychrome Hall* was 96.8±1.9% on average and ranged from 92% to 100%. In the outmost part of the cave (site C1), RH ranged from 88% to 100% and averaged 96.5±2.3% (Fig. 3E). Generally, the lowest RH values correspond to the cave ventilation period and values closer to 100% are characteristic of the stagnation period. The RH in the inner cave sector is slightly higher and closer to saturation (>97%), with no significant seasonal changes (Gázquez et al., 2016; Sainz et al., 2018).

4.4. Results of isotope modeling

The modeled $\delta^{18}O$ and δD values of condensation water for the sectors near the cave entrance (site C1) show a seasonal pattern, with higher values (up to -2.9‰ and -8.4‰, respectively) during the cave ventilation period and lower values during the stagnation period (down to -6.9‰ and -43.7‰, respectively) (Fig. 1). The modeled d-excess values of condensation water ranges from 10.1 to 16.2 ‰, with the lowest values corresponding to the ventilation period and higher values are obtained for the stagnation period. We found that the expected range of ^{17}O-excess in condensation water is only of 9 per meg. Note that this variability is smaller than the analytical precision of our ^{17}O-excess measurements (~13 per meg). The highest ^{17}O-excess values occur during the cave stagnation period (maximum value of 28 per meg) and lower values are observed during the cave ventilation period (minimum of 19 per meg).

We tested the sensibility of the isotopic composition of condensation water to the different parameters consider by our model (external air temperature and cave atmosphere temperature, the isotopic composition of cave dripwater and meteoric

448 water and the degree of cave atmosphere ventilation). As expected, we found that
449 during the cave stagnation period the isotopic composition of condensation water at
450 site C1 is insensitive to changes in the outside air temperature and variations in the
451 isotopic composition of meteoric water (Supplementary Fig. 1 and 3). Also, changes
452 in the cave atmosphere temperature during the stagnation period have an insignificant
453 impact on the isotopic composition of condensation water (Supplementary Fig. 2),
454 given the small temperature variations in the cave atmosphere temperature (<5 ^{o}C).
455 In contrast, the isotopic composition of condensation water at site C1 during the cave
456 ventilation period is relatively sensitive to the changes in the external air temperature
457 (e.g. 1‰ δ^{18}O increase for each increment of 10 ^{o}C) (Supplementary Fig. 1). We found
458 that the δ^{18}O and δD values of condensation increase linearly with the δ^{18}O and δD
459 values of the external meteoric water (Supplementary Fig. 3), while changes in the
460 cave temperature atmosphere have little impact on the δ^{18}O and δD values of
461 condensation water (e.g. 0.2‰ δ^{18}O increase for an increment of 2 ^{o}C)
462 (Supplementary Fig. 2). Likewise, the secondary parameters d-excess and ^{17}O-excess
463 are insensitive to change in the external parameters during the cave stagnation period
464 (Supplementary Figures 1 to 3). In contrast, during the ventilation period, the d-excess
465 of condensation water in the outmost cave sectors is significantly impacted by changes
466 the external air temperature (i.e. 3.7‰ d-excess increase for each increment of 10 ^{o}C)
467 and by changes in the d-excess of meteoric water. The modeled ^{17}O-excess values of
468 condensation water at site C1 during the ventilation period are barely affected by
469 changes in the internal and external air temperatures (i.e. 1 per meg increase for each
470 increment of 10 ^{o}C).
471

5. Discussion

The difference in isotopic composition of two water reservoirs (e.g. liquid and vapor) in equilibrium during phase change depends mostly on temperature that controls the equilibrium isotope fractionation factors between the two phases (e.g. $\alpha^{18}O_{water\text{-}vapor}$ and $\alpha D_{water\text{-}vapor}$) (Craig et al., 1963; Horita and Wesolowski, 1994). Additionally, when the evaporation-condensation process occurs under RH<100%, kinetic isotope fractionation can take place, which magnitude depends mostly on relative humidity and the degree of turbulence on the liquid-vapor boundary layer (i.e. wind) (Cappa et al., 2003; Landais et al., 2006; Barkan and Luz, 2007, Luz et al., 2009). In caves, relative humidity is close to 100% (e.g. Fig. 2) and wind speed is generally insignificant compared to outside (Gázquez et al., 2016); thus, equilibrium isotope process is expected to prevail over kinetic isotope fractionation during phase changes. Consequently, for the particular case of condensation in caves, the most important parameters controlling the isotopic composition of condensation water are temperature and the isotopic composition of water vapor.

Our monitoring data show that Altamira Cave directly, and rapidly, exchanges gases with the external atmosphere during the cave ventilation period (June to October), when intakes of water vapor from outside are expected. Note that the seasonal environmental changes outside are considerably larger than in the cave. This includes larger temperature changes and varying isotopic of compositions of water vapor. Indeed, the isotopic composition of summer rainfall in this region is more enriched (e.g. $\delta^{18}O$~-3.5‰ in June) than in winter (e.g. $\delta^{18}O$~-6.7‰ in January) (IAEA/WMO 2021) and external water vapor is assumed here to be in equilibrium with environmental liquid water outside. According to this, the isotopic composition of atmospheric vapor outside the cave during summer is expected to increase compared to winter

conditions. In contrast, the isotopic composition of the autochthonous water vapor generated within the cave is expected to be less variable that outside because of cave temperature is nearly constant and the vapor is in equilibrium with the cave dripwater, which has almost constant isotopic values (Table 1 and Fig. 2). We evaluate the impact of allochthonous water vapor entering the cave during the ventilation period on the isotopic composition of condensation water at site C1 (*Entrance Hall*) by using a two-endmember mixing model (Fig. 2 and Supplementary Table 2).

The magnitude and variability of the modeled isotopic values for site C1 agree with our observations of $\delta^{18}O$ and δD of condensation water at site C1 (Fig. 2). Our model demonstrates that the seasonal cycles recorded by the isotopic composition of condensation water in the outmost part of the cave are a consequence of advection of allochthonous water vapor from the external atmosphere. The "summer condensation water" that accumulates during the ventilation period near the Entrance Hall is isotopically enriched (i.e. higher $\delta^{18}O$ and δD values) compared to the "winter condensation water" that derives from recycling of autochthonous water vapor generated in the cave water during the stagnation period (Figs. 3 and 5). The relatively constant $\delta^{18}O$ and δD values of autochthonous water vapor (ranges of 0.3‰ and 2.7‰, respectively) is a consequence of the small cave temperature variability and the almost constant isotopic values of seepage water through the seasonal cycle.

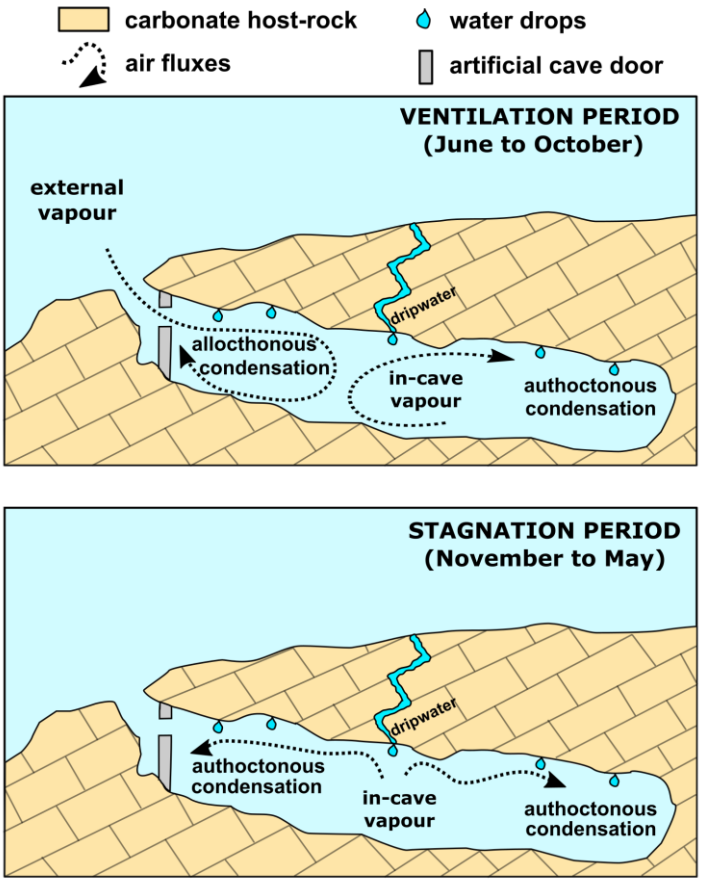

516

517 **Figure 5.** Conceptual diagram of condensation water systematic in Altamira Cave,
518 during the cave ventilation period (A) and the cave stagnation period (B). The inner
519 cave sectors are less affected by water vapor transported by air masses from outside
520 during the entire year, while the main source of vapor for condensation in these areas
521 is autochthonous water vapor generated from dripwater. The outmost areas receive
522 allochthonous water vapor from outside only during the ventilation period, while the
523 autochthonous vapor is the majority source of moisture for condensation in the entire
524 cave during the stagnation period. The metal door that separates the *Entrance Hall*
525 from the rest of the cave has been represented.

526

Condensation from allochthonous water vapor in caves seems to be analogue to recharge by “occult rain” detected in arid regions that occurs because of re-evaporation of local water and subsequent condensation of vapor on vegetation and soils (Aravena et al., 1989; Kaseke et al., 2017). If such vapor is re-condensed in any significant quantity before mixing with the larger tropospheric reservoir, the isotopic composition of the resulting condensation water will fall slightly above the LMWL (i.e. higher d-excess values), along a condensation line with a slope similar to the LMWL (Ingraham and Matthews, 1988, 1990; Clark and Fritz, 1997). Indeed, we found that y-intercept of the $\delta^{18}O$-δD correlation line of condensation water in the outmost part of the cave (site C1) is slightly higher (9.1±1.1‰) than that of the Local Meteoric Water Line (LMWL) (7.4±0.8‰), although their slopes are indistinguishable within errors (Fig. 3). Similarly, an offset between d-excess of condensation water and the LMWL has been observed in other caves (Gázquez et al., 2017b; Liñán et al., 2021).

Evaporation of condensation water can explain some of the d-excess outliers observed in the *Entrance Hall* that were recorded mostly during the cave ventilation period (e.g. three d-excess values ranging from 7 to 10.5‰ in summer 2017, 2018 and 2019; Fig. 4). These d-excess values are slightly lower than predicted by our model (Fig. 2C). Note that evaporated water normally show lower d-excess values (that correlates with $\delta^{18}O$ and δD) compared to non-evaporated waters (e.g. Luz et al., 2009; Gázquez et al., 2018; Voigt et al., 2021). However, the correlation between $\delta^{18}O$ and d-excess of condensation water in Altamira Cave is weak (R^2=0.28), the d-excess of condensation water remains generally high during the ventilation period (~15‰ and up to 17.3‰) and can occasionally show lower values during the rest of the year. In consequence, the seasonal variability of condensation water at site C1 cannot be

attributed to the effect of evaporation, but to the varying contributions of autochthonous and allocthonous water vapor.

The modeled ^{17}O-excess values of condensation water at site C1 vary from 19 per meg during the cave stagnation period to 28 per meg during the ventilation period (Fig. 2). No statistically significant seasonal trends in ^{17}O-excess of our analytical data have been observed in any of the sites investigated in this study, either in condensation water nor in dripwater. Recent studies showed that the δ^{18}O-^{17}O-excess relationship in rainwater in northern Spain (Villanua village, ~220 km from Altamira Cave) has a slope of 3.8 per meg/‰. Considering that the δ^{18}O of rainwater in Santander city varies seasonally by ~3‰, a range of ^{17}O-excess in rainwater of 12 per meg would expected. The expected ^{17}O-excess variability in dripwater of Altamira Cave is even smaller (2 per meg), considering the small δ^{18}O variability observed during the length of this study (0.5‰). Regarding that the mean reproducibility of our ^{17}O-excess measurements is 13 per meg (1SD), we conclude than the current analytical precision of the CRDS analyzers is insufficient to investigate the small ^{17}O-excess variability expected for condensation water and dripwater in caves.

As for condensation water in the inner cave sectors, the triple oxygen and hydrogen isotopic values in dripwater and its temporal variability (site D1) are indistinguishable from to those of condensation water collected from the inner cave sectors (sites C2 and C3). This suggests that water condensation from autochthonous water vapor in Altamira Cave cannot be differentiated from seepage water by using oxygen and hydrogen isotopes. Also, the isotopic composition of the ceiling droplets with no apparent dripping (sites D2, D3, D4 and D5) of the *Polychrome Hall* and the rest of condensation waters from the inner cave sectors (sites C2 and C3) show indistinguishable values within errors. No clear differences between the ventilation and

576 the stagnation periods has been identified. Thus, it is possible that the ceiling droplets
577 with of the *Polychrome Hall* are related to water condensation; however, contributions
578 of meteoric water infiltration and extremely slow drainage of the epikarst over this
579 chamber cannot be ruled out from our data.

580 We found that the small seasonal changes observed in the isotopic composition of
581 dripwater and condensation water in sectors relatively distant from the cave entrance
582 do not seem to be controlled by ventilation/stagnation regimen of the cave, since no
583 correlation with the CO_2 content or with in-cave air temperature has been observed
584 (Fig. 4). This indicates that the main source of vapor for condensation in these sites is
585 autochthonous water vapor from within the cave, with insignificant contributions of
586 allochthonous air masses, even during the ventilation period. This is probably related
587 to the fact that allochthonous water vapor condenses on cave surfaces closer to the
588 entrance and, likely on the artificial door that separates the *Entrance Hall* and the rest
589 of the cave, which is permanently closed. In consequence, the allochthonous water
590 vapor does not reach the inner cave sector even during the ventilation periods and
591 does not impact on the isotopic composition of condensation water in these areas.

592

593 **6. Conclusions**

594 We investigate the spatiotemporal variability of $\delta^{17}O$, $\delta^{18}O$, δD and derived ^{17}O-excess
595 and d-excess values of condensation water in Altamira Cave. Significant changes in
596 some of these parameters have been observed in the outmost cave sectors, while in
597 the inner/deeper cave parts the isotopic composition of condensation water is less
598 variable though the seasonal cycles. In particular, we found that the $\delta^{18}O$ and δD of
599 condensation water in the cave sectors closer to the entrance during the ventilation

600 period (June to October) are higher than during the stagnation period (November to
601 May). We evaluate the role of cave ventilation pattern in the condensation process in
602 this cave sector by using an isotope mixing model. We found that the isotopic
603 composition of condensation water near the cave entrance during the ventilation
604 period agrees with the expected values of water condensed from allochthonous water
605 vapor, while the prevailing mechanism during the stagnation period is condensation
606 from autochthonous water vapor generated within the cave.

607 Importantly, no significant differences have been found between the isotopic
608 composition of condensation water in the inner cave sectors and dripwater. This
609 suggests that the water condensation process in areas more distant from the cave
610 entrance is sourced by autochthonous water vapor. Given that the isotopic
611 composition of condensation water though the seasonal cycle is indistinguishable from
612 that of seepage water in the cave, we conclude that oxygen and hydrogen isotopes
613 are not useful in identifying the origin (condensation vs. seepage) of the droplets with
614 no apparent dripping that cover the ceiling of the *Polychrome Hall.* Also, we found that
615 the analytical precision of the current CRDS isotope analyzers to measure triple
616 oxygen isotope anomalies in waters is not enough to resolve the small seasonal
617 variations expected for cave waters (tens per meg).

618 The varying contributions of the allochthonous and autochthonous water vapor
619 sources for condensation in the cave can be attributed the natural cave ventilation, as
620 well as to the distance of the different chambers to the cave entrance and probably to
621 the role in the cave microclimate of the artificial metal door that separates the *Entrance*
622 *Hall* and the rest of the cave, as observed in previous studies (Gázquez et al., 2016;
623 Sainz et al., 2017). It is possible that a decrease in the airflow speed during the
624 ventilation period in this cave sector favors that water vapor from outside condenses

mostly in surfaces near the artificial door. Thus, this artificial element seems to be critical to prevent the *Polychrome Hall* and the rest of the cave from receiving additional water vapor from outside during the ventilation period. Our results are important for the management of the *Polychrome Hall*, since condensation water can contribute to the deterioration of the its exceptional rock art by washing out the ochre pigments. Additional efforts should be made to quantify and monitor condensation processes in Altamira Cave in forthcoming years.

Acknowledgments

The authors are grateful to the Altamira Cave Research Centre and Museum staff for their help and support during the sampling surveys in the cave. This work was supported by the Ministry of Education, Culture and Sport of Spain (MECD) [grant number J180052] under the Project “Servicio de control y seguimiento de las condiciones ambientales y del biodeterioro de la Cueva de Altamira”, and also with the support of the Cantabrian International Institute for Prehistoric Research (IIIPC) under the project entitled “Control y seguimiento de las condiciones ambientales, del agua de infiltración y de las emisiones de gas radon, de la cueva de Altamira”. The authors thanks Professor David A. Hodell for the isotopic analysis of 15 water samples. Dr. Fernando Gázquez was financially supported by the HIPATIA research program of the University of Almería and by a Ramón y Cajal Fellowship (RYC2020-029811-I) of the Spanish Government (Ministerio de Economía y Competividad). The authors are grateful to four anonymous reviews, who contributed to improve the original manuscript.

7. References

Aravena, R., Suzuki, O., Polastri, A., 1989. Coastal fogs and their relation to groundwater. Chem. Geol. 79, 83–91.

Aron, P. G., Levin, N.E., Beverly, E.J., Huth, T.E., Passey, B.H., Pelletier, E, M., Poulsen, C, J., Winkelstern, I., Yarian, D. 2021. Triple oxygen isotopes in the water cycle. Chem. Geol. 565(1):120026.

Auler, A.S., Smart, P.L., 2004. Rates of condensation corrosion in speleothems of semi-arid northeastern Brazil. Speleogenesis Evol. Karst Aquifers 2 (2) (2 pp.).

Barkan, E., Luz, B., 2005. High precision measurements of $^{17}O/^{16}O$ and $^{18}O/^{16}O$ ratios in H_2O. Rapid Commun. Mass Spectrom. 19, 3737–3742.

Barkan, E., Luz, B., 2007. Diffusivity fractionations of $H_2{}^{16}O/H_2{}^{17}O$ and $H_2{}^{16}O/H_2{}^{18}O$ in air and their implications for isotope hydrology. Rapid Commun. Mass Spectrom. 21, 2999–3005.

Bowen, G.J., Cai, Z., Fiorella, R.P., Putman, A.L., 2019. Isotopes in the Water Cycle: Regional- to Global-Scale Patterns and Applications. Ann. Rev. Earth Plant. Sci. 47, 453-479.

Calaforra, J.M., 1996. Contribución al conocimiento de la karstología de yesos (PhD Thesis). University of Granada, Spain (350 pp.).

Calaforra, J.M., Dell'Aglio, A., Forti, P., 1993. Preliminary data on the chemical erosion in gypsum karst. The Sorbas region (Spain). Proceedings of the 11th International Congress of Speleology (Beijing), pp. 97–99.

Cappa, C.D., Hendricks, M.B., DePaolo D.J., Cohen, R.C. 2003. Isotopic fractionation of water during evaporation. J. Geophys. Res., 108(D16), 4525.

672 Clark, I.D., Fritz, P., 1997. Environmental Isotopes in Hydrogeology. Lewis
673 Publishers, USA.

674 Craig, H., Gordon, L., Horibe Y., 1963. Isotopic exchange effects in the evaporation
675 of water: 1. Low-temperature experimental results. J. Geophys. Res. 68, 5079–
676 5087.

677 Cuezva, S., Sánchez-Moral, S., Saiz-Jiménez, C., Cañaveras, J.C., 2009. Microbial
678 communities and associated mineral fabrics in Altamira Cave. Spain. Int. J.
679 Speleol. 38 (1), 83-92.

680 Cuezva, S., Fernández-Cortés, A., Benavente, D., Serrano-Ortíz, P., Kowalski, A.S.,
681 Sánchez-Moral, S., 2011. Short-term CO_2(g) exchange between a shallow
682 karstic cavity and the external atmosphere during summer: Role of the surface
683 soil layer. Atmos. Environ. 45, 1418-1427.

684 De Freitas, C.R., Schmekal, A.A., 2003. Condensation as a microclimate process:
685 measurement, numerical simulation and prediction in the Glowworm tourist cave,
686 New Zealand. Int. J. Climatol. 23, 557–575.

687 De Freitas, C.R., Schmekal, A., 2006. Studies of corrosion/condensation process in
688 the Glowworm Cave, New Zealand. Int. J. Speleol. 35, 75–81.

689 Dreybrodt, W., Gabrovšek, F., Perne, M., 2005. Condensation corrosion: a
690 theoretical approach. Acta Carsol. 34, 317–348.

691 Dublyansky, V.N., Dublyansky, Y.V., 1998. The problem of condensation in karst
692 studies. J. Caves Karst Stud. 60 (1), 3–17.

693 Dublyansky, V.N., Dublyansky, Y.V., 2000. The role of condensation in karst
694 hydrogeology and speleogenesis. In: Klimchouk, A.B., Ford, D.C., Palmer, A.N.,

695 Dreybrodt, W. (Eds.), Speleogenesis, Evolution of Karst Aquifers. National
696 Speleological Society, Huntsville, pp. 100–111.

697 Elez, J., Cuezva, S., Fernández-Cortés, A., García-Antón, E., Benavente, D.,
698 Cañaveras, J.C., Sánchez-Moral, S., 2013. A GIS-based methodology to
699 quantitatively define an Adjacent Protected Area in a shallow karst cavity: case
700 of Altamira cave. J. Environ. Manage. 118, 122-124.

701 Fernández-Cortés, A., Calaforra, J.M., García-Guinea, J., 2006. The Pulpí gigantic
702 geode (Almería, Spain): geology, metal pollution, microclimatology and
703 conservation. Environ. Geol. 50, 707–716.

704 Gabrovšek, F., Dreybrodt, W., Perne, M., 2010. Physics of condensation corrosion
705 in caves. In: Andreo, B., Carrasco, F., Durán, J.J., LaMoreaux, J.W. (Eds.),
706 Advances in Research in Karst Media, Environmental Earth Sciences, pp. 491–
707 496.

708 Gázquez, F., Calaforra, J.M., Forti, P., DeWaele, J., Sanna, L., 2015a. The role of
709 condensation in the evolution of dissolutional forms in gypsum caves: study case
710 in the karst of Sorbas (SE Spain). Geomorphology, 229, 100–111.

711 Gázquez, F., I. Mather, J. Rolfe, N. P. Evans, D. Herwartz, M. Staubwasser, D. A.
712 Hodell., 2015b. Simultaneous analysis of $^{17}O/^{16}O$, $^{18}O/^{16}O$ and $^{2}H/^{1}H$ of gypsum
713 hydration water by cavity ringdown laser spectroscopy. Rapid Commun. Mass
714 Spectrom. 21, 1997–2006.

715 Gázquez, F. Quindós-Poncela, L., Sainz, C., Fernández, A., Fuentes, I., Celaya, S.,
716 2016. Spatiotemporal distribution of $\delta^{13}C$-CO_2 in a shallow cave and its potential
717 use as indicator of anthropic pressure. J. Environ. Manage. 180, 421 - 432.

718 Gázquez, F., Rull, F., Sanz-Arraz, A., Medina, J., Calaforra, J.M., de las Heras, C.,
719 Lasheras, J.A., 2017a. In situ Raman characterization of minerals and
720 degradation processes in a variety of cultural and geological heritage sites.
721 Spetrochim. Acta Part B. 172, 48-57.

722 Gázquez, F., Calaforra, J.M., Evans, N.P., Hodell, D.A., 2017b. Using stable isotopes
723 (δ ^{17}O, δ ^{18}O and δD) of gypsum hydration water to ascertain the role of water
724 condensation in the formation of subaerial gypsum speleothems. Chem. Geol.
725 452, 34–46.

726 Gázquez, F., Morellón, M., Bauska, T., Herwartz, D., Surma, J., Moreno, A.,
727 Staubwasser, M., Valero-Garcés, B., Delgado-Huertas, A., Hodell, D.A., 2018.
728 Triple oxygen and hydrogen isotopes of gypsum hydration water for quantitative
729 paleo-humidity reconstruction. Earth Planet. Sci. Lett. 481, 177–188.

730 García-Antón, E., Cuezva, S., Jurado, V., Porca, E., Miller, A.Z., Fernández-Cortés,
731 A., Saiz-Jiménez, C., Sánchez-Moral, S., 2013. Combining stable isotope (δ^{13}C)
732 of trace gases and aerobiological data to monitor the entry and dispersion of
733 microorganisms in caves. Environ. Sci. Poll. Res. 21, 473-484.

734 García-Antón, E., Cuezva, S., Fernández-Cortés, A., Benavente, D., Sánchez-Moral,
735 S., 2014. Main drivers of diffusive and advective processes of CO_2-gas exchange
736 between a shallow vadose zone and the atmosphere. Int. J. Greenh. Gas. Con.
737 21, 113-129.

738 Giménez, R. Bartolomé, M., Gázquez, F., Iglesias, M., Moreno, A. 2021. Underlying
739 climate controls in triple oxygen (^{16}O, ^{17}O, ^{18}O) and hydrogen (^{1}H, ^{2}H) isotopes
740 composition of rainfall (Central Pyrenees). Front. Earth Sci. 9, 633698.

741 Horita, J., Wesolowski, D.J., 1994. Liquid–vapor fractionation of oxygen and
742 hydrogen isotopes of water from the freezing to the critical temperature.
743 Geochim. Cosmochim. Acta 58, 3425–3437.

744 Hoyos, M., Bustillo, A., Garcia, A., Martin, C., Ortiz, R., Suazo, C., 1981.
745 Características geológico-kársticas de la cueva de Altamira (Santillana del Mar,
746 Santander). Informe Ministerio de Cultura, Madrid, 81 pp.

747 IAEA/WMO (2021). Global Network of Isotopes in Precipitation. The GNIP Database.
748 Accessible at: http://www.iaea.org/water.

749 Ingraham, N.L., Matthews, R.A., 1988. Fog drip as a source of groundwater recharge
750 in northern Kenya. Water Resour. Res. 24, 1406–1410.

751 Ingraham, N.L., Matthews, R.A., 1990. A stable isotopic study of fog: the Point Reyes
752 Peninsula, California, U.S.A. Chem. Geol. 80, 281–290.

753 Kaseke, K.F., Wang, L., Seely M.K. 2017. Nonrainfall water origins and formation
754 mechanisms. Sci. Adv. 3, e1603131.

755 Klimchouk, A.B., 1996. Speleogenesis in gypsum. Int. J. Speleol. 25 (3–4), 61–82.

756 Klimchouk, A.B., Aksem, S.D., 2002. Gypsum karst in the western Ukraine:
757 Hydrochemtry and solution rates. Carbonate Evaporite 17, 142–153.

758 Landais, A., Barkan, E., Yarik, D., Luz, B., 2006. The triple isotopic composition of
759 oxygen in leaf water. Geochim. Cosmochim. Acta. 70, 4105-4115.

760 Liñan, C., Benavente, J., del Rosal, Y., Vadillo, I., Ojeda, L., Carrasco, F., 2021.
761 Condensation water in heritage touristic caves: isotopic and hydrochemical data
762 and a new approach for its quantification through image analysis. Hydrolocial
763 Processes. doi: 10.1002/hyp.14083. in press.

764 Luz, B., Barkan, E., 2005. The isotopic ratios $^{17}O/^{16}O$ and $^{18}O/^{16}O$ in molecular
765 oxygen and their significance in biogeochemistry. Geochim. Cosmochim. Acta
766 69, 1099–1110.

767 Luz, B., Barkan, E., 2010. Variations of $^{17}O/^{16}O$ and $^{18}O/^{16}O$ in meteoric waters.
768 Geochim. Cosmochim. Acta 74, 6276–6286.

769 Luz, B., Barkan, E., Yam, R., Shemesh, A., 2009. Fractionation of oxygen and
770 hydrogen isotopes in evaporating water. Geochim. Cosmochim. Acta 73, 6697–
771 6703.

772 Pike, A.W.G., Hoffmann, D.L., García-Idez, M., Pettitt, P. B., Alcolea, J., Balbín, R.D.,
773 Gónzalez-Saiz, C., De las Heras, C., Lasheras, J.A., Montes, R., Zilhao, J., 2012.
774 U-Series Dating of Paleolithic Art in 11 Caves in Spain. Science 336 (6087),
775 1409-1413.

776 Uechi, Y., and Uemura, R., 2019. Dominant influence of the humidity in the moisture
777 source region on the 17O-excess in precipitation on a subtropical island. Earth
778 Planet. Sci. Lett. 513, 20–28.

779 Quindós, L.S., Bonet, A., Daz-Caneja, N., Fernandez, P.L., Gutierrez, I., Solana, J.R.
780 Soto, J., Villar, E., 1987. Study of the environmental variables affecting the
781 natural preservation of the Altamira Cave paintings located at Santillana del Mar,
782 Spain. Atmos. Environ. 21(3), 551-560.

783 Sainz, C., Rábago, D., Celaya, S., Fernandez, E., Quindós, J., Quindós, L,
784 Fernández, A., Fuente, I., Arteche, J.L., Quindós, L.S., 2017. Continuous
785 monitoring of radon gas as a tool to understand air dynamics in the cave of
786 Altamira (Cantabria, Spain). Sci. Total Environ. 624, 416-423.

Sarbu, S.M., Lascu, C., 1997. Condensation Corrosion in Movile Cave, Romania. J. Caves Karst Stud. 59, 99–102.

Schoenemann, S. W., Schauer, A. J., Steig, E. J., 2013. Measurement of SLAP2 and GISP $\delta^{17}O$ and proposed VSMOW-SLAP normalization for $\delta^{17}O$ and $^{17}O_{excess}$. Rapid Commun. Mass Spectrom. 27, 582–590.

Steig, E. J., Gkinis, V., Schauer, A. J., Schoenemann, S. W., Samek, K., Hoffnagle, J., Dennis K.J., Tan, S.M., 2014. Calibrated high-precision ^{17}O-excess measurements using cavity ring-down spectroscopy with laser-current-tuned cavity resonance. Atmos. Meas. Tech. 7, 2421–2435.

Surma, J., Assonov, S., Staubwasser, M., 2021. Triple Oxygen Isotope Systematics in the Hydrologic Cycle. Rev. Mineral. Geochem. 86(1):401-428.

Tarhule-Lips, R.F.A., Ford, D.C., 1998. Condensation corrosion in caves on Cayman Brac and Isla de Mona. J. Caves Karst Stud. 60, 84–95.

Tian, C., Wang, L., Kaseke, K.F., Bird, B.W., 2018. Stable isotope compositions (d2H, d18O and d17O) of rainfall and snowfall in the central United States. Sci. Rep. 8, 6712.

Voigt, C., Herwartz, D., Dorador, C., Staubwasser, M. 2021. Triple oxygen isotope systematics of evaporation and mixing processes in a dynamic desert lake system. Hydrol. Earth Syst. Sci., 25, 1211–1228.

Wassenaar, L., Terzer-Wassmuth, S., Douence, C. Progress and challenges in dual- and triple-isotope (δ18O, δ2H, Δ17O) analyses of environmental waters: An international assessment of laboratory performance. Rapid Commun Mass Spectrom. 35(24):e9193.

White, J.H., Dominguez-Villar, D., Hartland, A., 2021. Condensation corrosion alters the oxygen and carbon isotope ratios of speleothem and limestone surfaces. Res. Geochem., e100008.

Figure 1

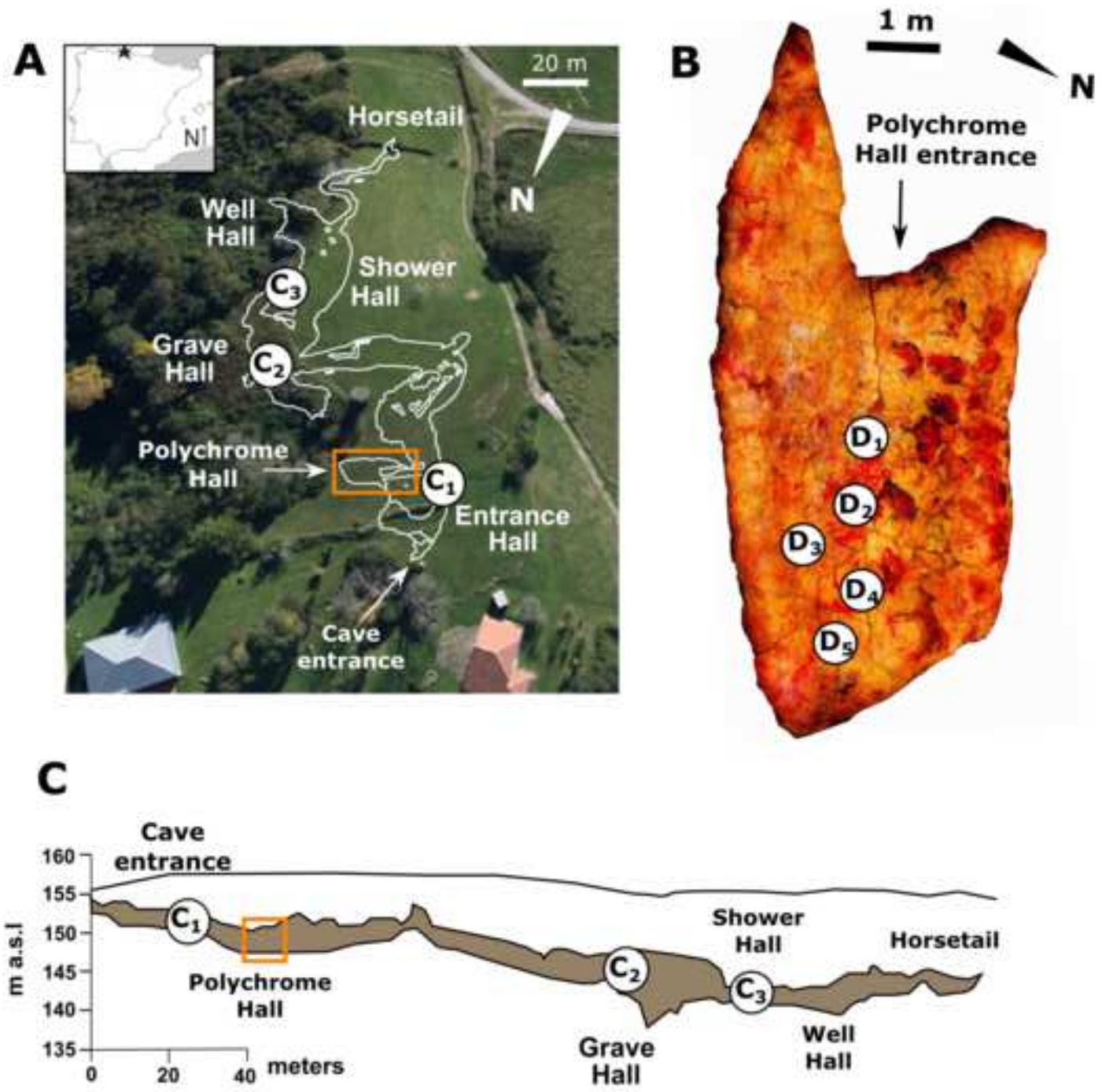

Figure 2

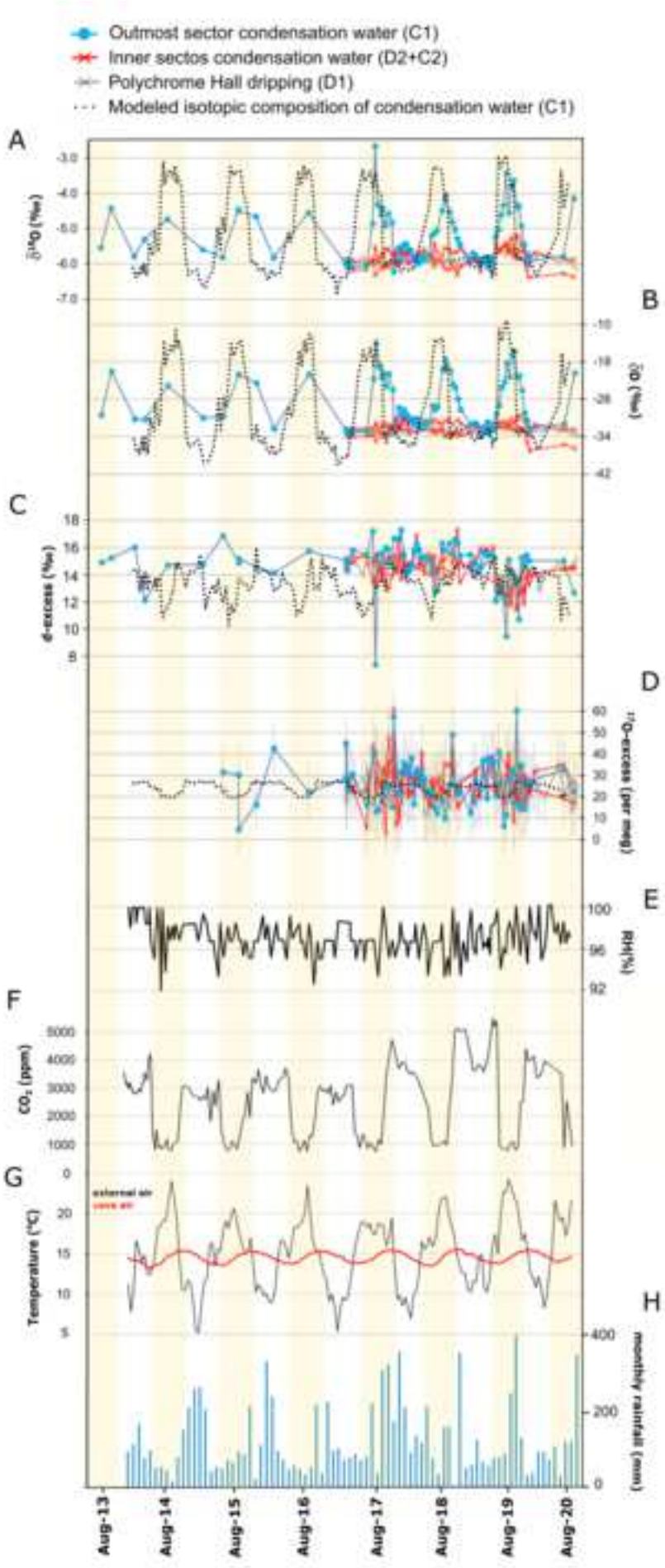

Figure 3

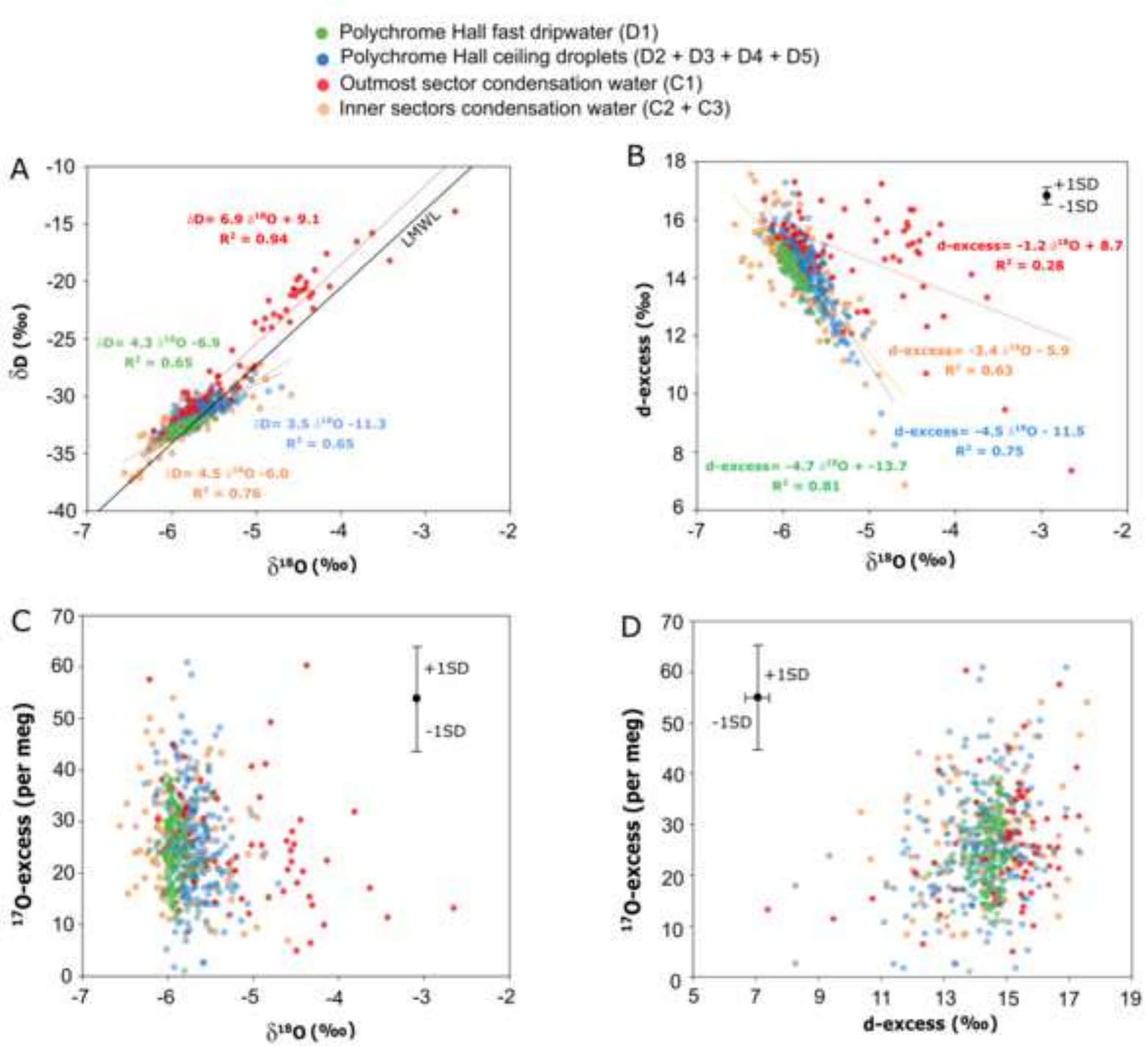

Figure 4

Click here to access/download;Figure;Figure 4 new.png

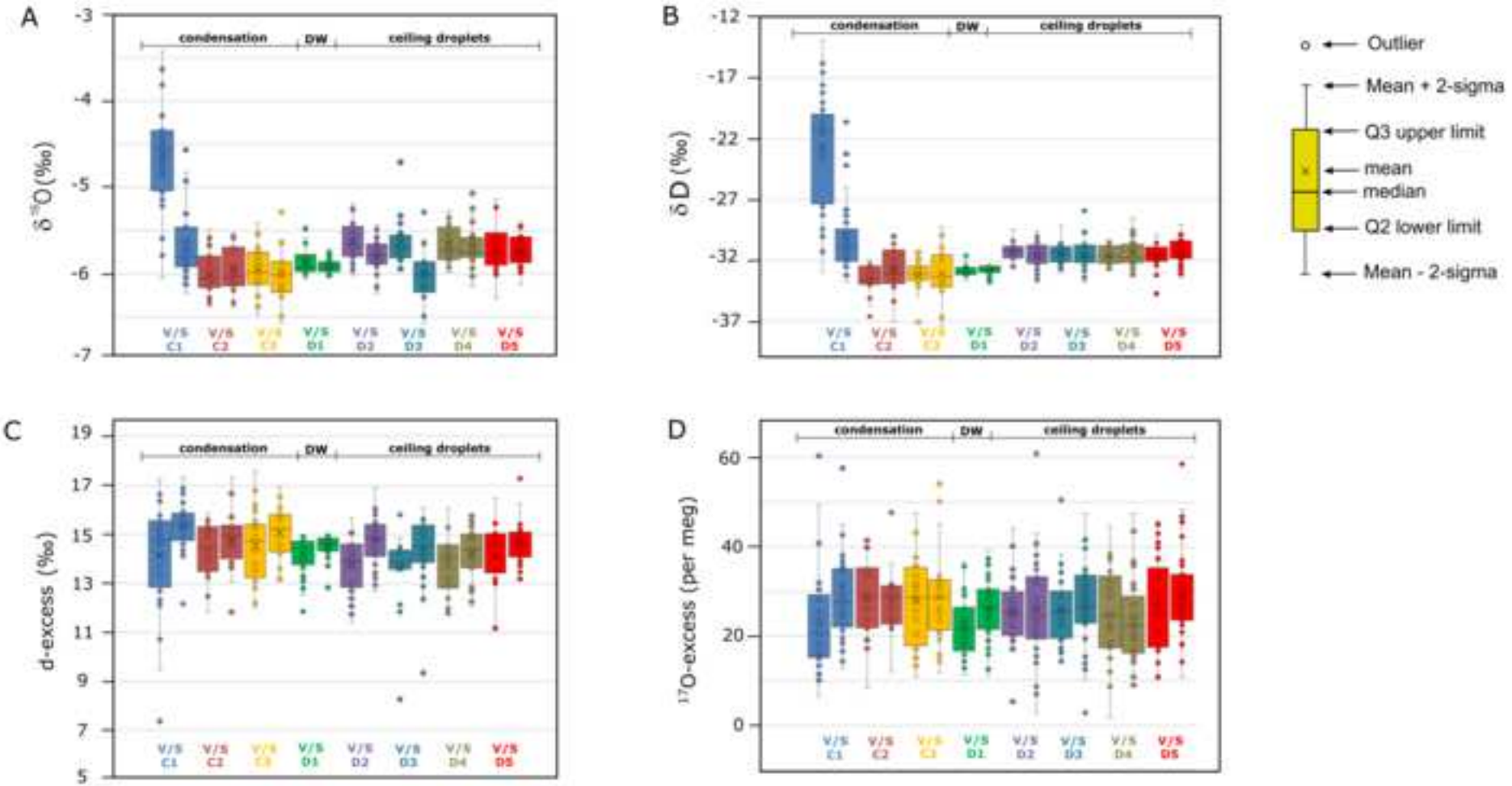

Figure 5

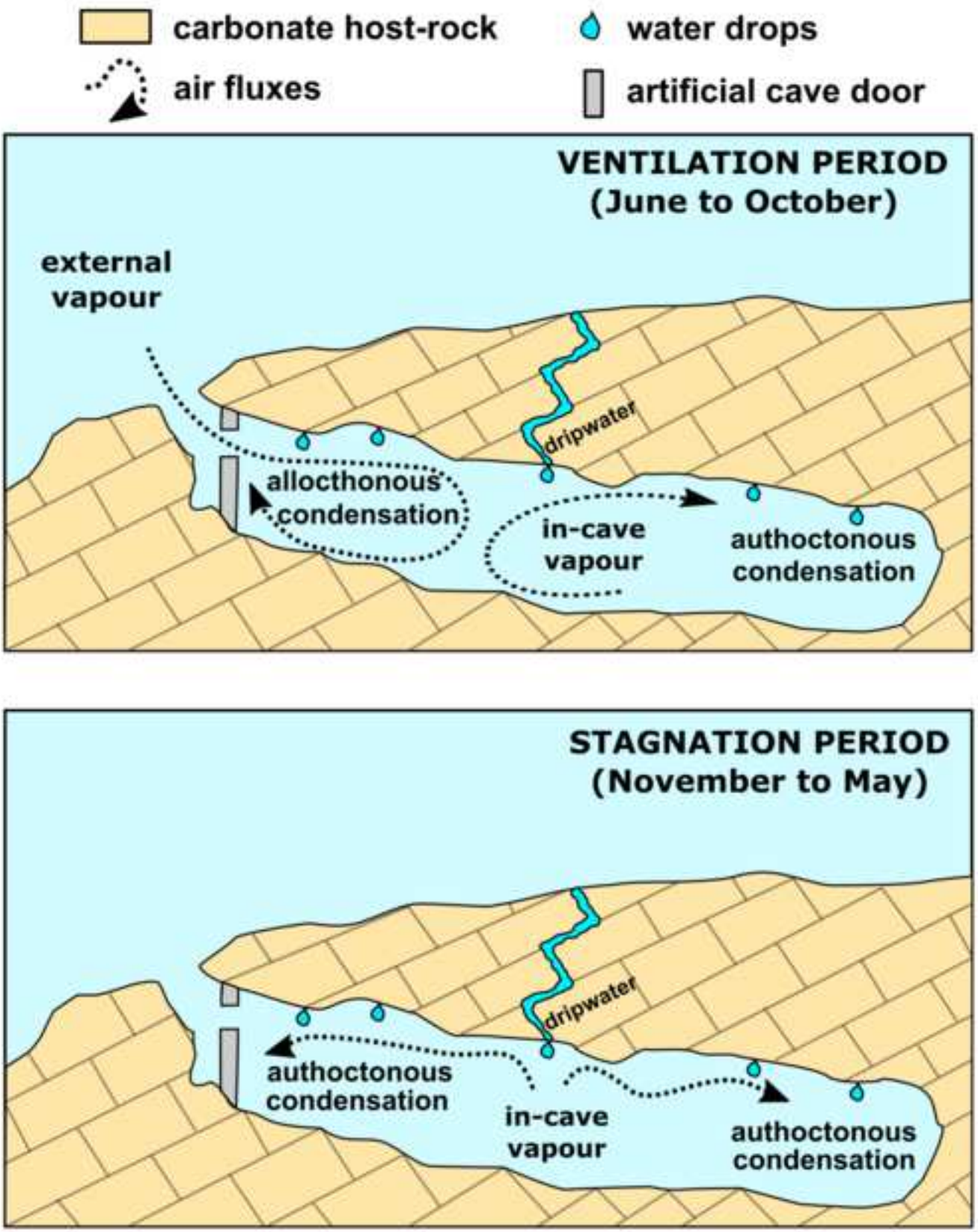

Table 1

Sampling site	Location code*	Period	Type	V/S	$\delta^{17}O$ (‰) ± 1SD	$\delta^{17}O$ (‰) max	$\delta^{17}O$ (‰) min	$\delta^{18}O$ (‰) ± 1SD	$\delta^{18}O$ (‰) max	$\delta^{18}O$ (‰) min	δD (‰) ± 1SD	δD (‰) max	δD (‰) min	d-excess (‰) ± 1SD	d-excess (‰) max	d-excess (‰) min	^{17}O-excess (per meg) ± 1SD	^{17}O-excess (per meg) max	^{17}O-excess (per meg) min
Entrance Hall	C1	15/07/2013 to 12/08/2020	Condensation on artificial support	V	-2.39 ±0.37	-1.39	-3.18	-4.60 ±0.69	-2.66	-6.05	-22.4 ±4.6	-13.9	-32.7	14.3 ±2.1	17.2	7.4	27 ±12	60	7
				S	-2.96 ±0.21	-2.96	-3.23	-5.65 ±0.40	-4.56	-6.22	-30.0 ±3.0	-20.6	-32.7	15.2 ±1.1	17.3	12.1	28 ±9	58	13
Middle Sector	C2	13/03/17 to 12/08/2020	Condensation on artificial support	V	-3.14 ±0.13	-2.87	-3.36	-5.99 ±0.25	-5.49	-6.38	-33.5 ±1.2	-31.9	-36.6	14.3 ±1.1	15.8	11.8	28 ±9	42	8
				S	-3.12 ±0.14	-2.90	-3.35	-5.95 ±0.26	-5.53	-6.39	-32.7 ±1.9	-29.9	-37.0	14.8 ±1.2	17.3	11.8	29 ±8	48	12
Great Hall	C3	13/03/17 to 12/08/2020	Condensation on artificial support	V	-3.14 ±0.13	-2.84	-3.40	-5.99 ±0.25	-5.42	-6.47	-33.3 ±1.1	-31.3	-37.1	14.6 ±1.3	17.6	12.0	26 ±10	47	11
				S	-3.13 ±0.16	-2.78	-3.44	-5.97 ±0.31	-5.29	-6.56	-32.8 ±2.0	-29.2	-37.3	14.9 ±1.2	16.9	12.8	30 ±11	54	12
Polychrome Hall	D1	13/03/17 to 12/08/2020	Dripwater	V	-3.08 ±0.08	-2.86	-3.18	-5.87 ±0.14	-5.48	-6.05	-32.8 ±0.4	-31.6	-33.6	14.1 ±0.8	14.9	11.9	22 ±7	36	11
				S	-3.10 ±0.04	-3.00	-3.16	-5.91 ±0.07	-5.71	-6.02	-32.8 ±0.4	-32.2	-33.7	14.5 ±0.4	15.0	12.8	26 ±7	39	11
Polychrome Hall	D2	22/03/17 to 12/08/2020	Droplets on the cave ceiling	V	-2.95 ±0.12	-2.73	-3.18	-5.63 ±0.23	-5.20	-6.02	-31.2 ±0.85	-29.4	-32.5	13.9 ±1.1	15.7	11.4	25 ±9	44	5
				S	-3.03 ±0.10	-2.83	-3.26	-5.78 ±0.19	-5.36	-6.22	-31.5 ±0.9	-29.6	-33.7	14.7 ±1.1	16.9	12.1	26 ±11	61	3
Polychrome Hall	D3	22/03/17 to 12/08/2020	Droplets on the cave ceiling	V	-2.96 ±0.14	-2.47	-3.12	-5.64 ±0.26	-4.71	-5.96	-31.5 ±0.8	-29.2	-33.0	13.7 ±1.4	15.8	8.3	25 ±8	51	14
				S	-3.00 ±0.13	-2.55	-3.21	-5.73 ±0.25	-4.86	-6.14	-31.5 ±1.1	-27.9	-33.8	14.3 ±1.3	16.1	9.3	27 ±9	47	3
Polychrome Hall	D4	22/03/17 to 12/08/2020	Droplets on the cave ceiling	V	-2.98 ±0.10	-2.78	-3.14	-5.69 ±0.19	-5.27	-5.98	-31.5 ±0.74	-30.4	-32.7	13.9 ±1.1	16.0	11.7	25 ±11	45	2
				S	-2.98 ±0.12	-2.67	-3.20	-5.68 ±0.23	-5.07	-6.14	-31.3 ±1.1	-28.5	-33.3	14.1 ±1.1	15.8	12,9	23 ±9	47	9
Polychrome Hall	D5	22/03/17 to 12/08/2020	Droplets on the cave ceiling	V	-3.01 ±0.12	-2.72	-3.28	-5.75 ±0.22	-5.23	-6.27	-31.7 ±1.0	-30.4	-34.7	14.3 ±1.1	16.5	11.2	27 ±10	45	10
				S	-2.99 ±0.11	-2.70	-3.20	-5.72 ±0.21	-5.14	-6.12	-31.2 ±1.0	-29.1	-33.4	14.5 ±1.0	17.3	11.1	29 ±10	59	11

Table 1. Summary of triple oxygen and hydrogen isotopes in waters from Altamira Cave (*see Figure 1 for sampling site locations). Results of the cave ventilation period (V; June to October) and stagnation period (S; November to May) are averaged.

Supplementary Table 1

Supplementary Table 2

Supplementary Table 3

Supplementary Figures 1, 2 and 3